AIMS Mathematics, 10(6): 13594–13621.
DOI:10.3934/math.2025612
Received: 07 March 2025
Revised: 29 May 2025
Accepted: 29 May 2025
Published: 13 June 2025

https://www.aimspress.com/journal/Math

Research article

Chaos, control and synchronization in discrete time computer virus system with fractional orders

Omar Kahouli[1,*], **Imane Zouak**[2], **Ma'mon Abu Hammad**[3] **and Adel Ouannas**[4]

[1] Department of Electronics Engineering, Applied College, University of Ha'il, Ha'il 2440, Saudi Arabia
[2] System Dynamics and Control Laboratory, Department of Mathematics and Informatics, University of Larbi Ben M'hidi, Oum El Bouaghi 04000, Algeria
[3] Department of Mathematics, Al-Zaytoonah University of Jordan, Amman 11733, Jordan
[4] Department of Mathematics and Computer Sciences, University of Larbi Ben M'hidi, Oum El Bouaghi 04000, Algeria

* **Correspondence:** Email: omarkahouli@yahoo.fr.

Abstract: In this research, we present a novel discrete fractional-order model designed to simulate computer virus propagation. We performed a thorough dynamical analysis, encompassing phase portrait visualization, bifurcation diagram construction, maximal Lyapunov exponent computation, and equilibrium point stability assessment using the basic reproduction number (R_0). To characterize system complexity and validate chaotic dynamics, we employed Approximate Entropy, C_0 Complexity, and Permutation Entropy. Furthermore, control and synchronization methodologies were developed to mitigate chaotic behavior and achieve coordinated system dynamics. The findings proved the efficacy of the proposed fractional model in accurately simulating viral spread and illustrated the considerable implications of fractional-order parameters on system dynamics. In order to validate the results, MATLAB simulations were run.

Keywords: computer viruses dynamics; fractional discrete model; stability; chaos; control
Mathematics Subject Classification: 34A08, 37D45, 68M12, 93C55, 93D20

1. Introduction

Computer viruses originated in the 1970s as malicious software programs designed to replicate themselves and spread through inter-computer transmission, with potential for data compromise and system instability and disrupting normal operations [1]. These viruses can infect files, alter system settings, and compromise data integrity and confidentiality [2]. Computer viruses pose significant

threats to cybersecurity, requiring vigilant measures such as antivirus software and regular updates to protect against them. Understanding their behavior and how they spread is crucial for safeguarding digital systems and sensitive information from potential harm [3].

The analogy between computer and biological viral propagation, particularly in terms of infectivity, has led researchers to modify established epidemiological models for the purpose of simulating computer virus propagation [4]. These models enable researchers to simulate and predict how computer viruses spread over time across networks, similar to how biological viruses spread within populations [5]. By applying these models, insights can be gained into viable tactics for mitigating and restricting the dissemination of computer viruses [6].

Chaos theory is an interdisciplinary area of study, primarily in math and physics, that examines the dynamics of systems exhibiting extreme sensitivity to initial states, meaning minute initial perturbations may result in significantly divergent results [7–9]. This makes their behavior seem random and hard to predict. It can be found in various fields like meteorology, biology, economics, and engineering to help explain and predict complex and dynamic behaviors [10]. The successful application of chaotic systems in secure communications, leveraging their complexity and sensitivity, provides a strong precedent for exploring their role in other security domains. For example, chaotic maps combined with neural networks enhance video encryption [11], while chaos theory and semi-tensor product theory secure face recognition [12]. These advancements, alongside developments in chaotic encryption, key distribution, and watermarking, underscore the potential of chaotic dynamics for significant security enhancements across various applications, thus motivating its investigation in the context of computer virus defense.

Fractional chaotic systems, which extend traditional chaotic systems by employing fractional calculus, offer unique advantages over both discrete and continuous chaotic systems [13–15]. Fractional calculus enables the use of non-integer order derivatives and integrals [16–18], providing greater flexibility and accuracy in modeling real-world phenomena [19–21]. This approach exhibits the potential to model both the memory and hereditary traits of systems, making fractional chaotic systems highly effective in fields such as control theory, digital signal manipulation, and bioengineering [22–24]. Understanding the benefits of fractional chaotic systems can lead to more precise and comprehensive models in complex systems [25–27]. In the context of computer virus modeling, fractional-order systems are particularly beneficial due to their ability to capture the memory effects inherent in network interactions. Unlike classical integer-order models, fractional-order models incorporate memory and hereditary properties, making them more suitable for describing complex systems such as computer virus propagation, which often exhibits delay and nonlocal behavior. However, this added realism comes at a cost. The analysis of fractional-order systems is significantly more challenging due to the lack of standard techniques for stability and control. Moreover, parameter estimation and numerical simulations are more computationally intensive, and the interpretation of fractional-order parameters in real applications remains an open question. Therefore, fractional-order modeling in this context is not merely a formal extension but introduces new theoretical and practical challenges that require careful mathematical treatment. In addition to their application in virus propagation models, fractional and discrete chaotic dynamics have also been successfully employed in secure communication systems. For example, chaotic maps have been used for image encryption in recent studies [28, 29], demonstrating the interdisciplinary potential of these systems in cybersecurity, where the inherent unpredictability and sensitivity to initial conditions provide

significant advantages. Existing methods for modeling chaotic systems and virus propagation, such as integer-order and discrete-time models, often overlook memory and hereditary effects. Fractional-order models, however, address these limitations by incorporating these effects, offering more accurate and flexible representations of real-world phenomena. This paper introduces a fractional-order approach, which provides enhanced control over virus dynamics, making it more suitable for real-time applications, especially in cybersecurity.

In the field of computer virus modeling, discrete-time approaches have been less explored compared to continuous-time methods [30]. However, discrete systems offer several practical advantages, particularly in the context of digital systems where time-stepping data is prevalent. These systems reduce the parametric sensitivity challenges often seen in continuous models, making them more stable and easier to implement. Furthermore, discrete models are well-suited for digital hardware implementations, offering simplicity and efficiency, which makes them ideal for real-time applications such as improving cybersecurity defenses against the rapidly evolving nature of computer viruses.

Here, we aim to present a thorough analysis of stability and dynamical properties of a novel model employing commensurate fractional derivatives. Researchers have extensively studied the stability and control of various computer virus models [31,32]. In this paper, we propose a novel discrete fractional-order model tailored to simulate the spread of computer viruses and explore the emergence of chaotic dynamics within such systems, a topic that has received limited attention in the discrete-time fractional framework. Here is a summary of the objectives in our work:

1) We introduce a new discrete fractional model developed to simulate the spread of computer viruses.
2) The long-term stability of the system is investigated by examining its equilibrium points.
3) A full examination of the dynamic attributes of the model by the agency of phase portraits, bifurcation diagrams, and maximum Lyapunov exponent calculations, is performed.
4) Complexity measures, specifically Approximate Entropy, C_0 Complexity, and Permutation Entropy, are used to evaluate complexity and verify chaos in the hypothesized fractional discrete model of computer viruses.
5) Additionally, control and synchronization strategies are implemented to stabilize the system and achieve coordinated behavior between chaotic maps.

In conclusion, we outline the key findings emerge from our study.

Unlike primarily focus on continuous-time or integer-order models (e.g., [6, 30]), we provide new insights into the behavior of commensurate fractional-order discrete-time systems, highlighting the rich dynamics and potential for chaos. One of the major challenges in this study was handling the intricate nature of fractional-order difference equations, especially in the context of chaos and control design. Our model and methods extend the theoretical framework to discrete settings, which are crucial for numerical implementation and digital systems. The results presented here therefore contribute both theoretical and practical value to the modeling and control of digital epidemic systems.

2. Fundamental tools and model

We will clarify our work by first presenting a focused review of discrete fractional calculus. Following this, we will unveil the mathematical description of the fractional discrete computer virus model, which is built through the application of the Caputo difference operator.

2.1. Fundamental tools

Let us dive into the scope of discrete fractional difference and summation from a different perspective. In all of the definitions below, the function $\mathscr{X}$ is defined for $\mathbb{N}_{\mathtt{a}}$, where $\mathbb{N}_{\mathtt{a}} = \{\mathtt{a}, \mathtt{a}+1, \mathtt{a}+2, \ldots\}$ for $\mathtt{a} \in \mathbb{R}$.

Definition 1. *[33] The Caputo-like fractional difference operator ${}^{\mathtt{c}}\Delta_{\mathtt{a}}^{\kappa}$ for a function $\mathscr{X}(\mathtt{t}) : \mathbb{N}_{\mathtt{a}} \to \mathbb{R}$ is defined as:*

$$ {}^{\mathtt{c}}\Delta_{\mathtt{a}}^{\kappa}\mathscr{X}(\mathtt{t}) = \Delta_{\mathtt{a}}^{-(\mathtt{m}-\kappa)}\Delta^{\mathtt{m}}\mathscr{X}(\mathtt{t}) = \frac{1}{\Gamma(\mathtt{m}-\kappa)} \sum_{\mathtt{b}=\mathtt{a}}^{\mathtt{t}-(\mathtt{m}-\kappa)} (\mathtt{t}-\mathtt{b}-1)^{(\mathtt{m}-\kappa-1)}\Delta^{\mathtt{m}}\mathscr{X}(\mathtt{b}), \mathtt{t} \in \mathbb{N}_{\mathtt{a}+\mathtt{m}-\kappa}, $$

where $\kappa > 0$ is the fractional order, $\mathtt{m} = \lceil\kappa\rceil + 1$, $\Gamma(\cdot)$ denotes the Gamma function that generalizes the factorial to real and complex numbers, and ${}^{\mathtt{c}}\Delta_{\mathtt{a}}^{-\kappa}$ is the κ-th fractional sum, which is outlined in [34] by:

$$ {}^{\mathtt{c}}\Delta_{\mathtt{a}}^{-\kappa}\mathscr{X}(\mathtt{t}) = \frac{1}{\Gamma(\kappa)} \sum_{\mathtt{b}=\mathtt{a}}^{\mathtt{t}-\kappa} (\mathtt{t}-\mathtt{b}-1)^{\kappa-1}\mathscr{X}(\mathtt{b}), \mathtt{t} \in \mathbb{N}_{\mathtt{a}+\kappa}, $$

the power term $(\mathtt{t}-\mathtt{b}-1)^{(\kappa-1)}$ is defined via the Gamma function as:

$$ (\mathtt{t}-\mathtt{b}-1)^{(\kappa-1)} = \frac{\Gamma(\mathtt{t}-\mathtt{b})}{\Gamma(\mathtt{t}-\mathtt{b}+1-\kappa)}. $$

Theorem 1. *[13] The solution of the fractional difference equation system:*

$$ \begin{cases} {}^{\mathtt{c}}\Delta_{\mathtt{a}}^{\kappa}\mathscr{Y}(\mathtt{t}) = \mathscr{X}(\mathtt{t}+\kappa-1, \mathscr{Y}(\mathtt{t}+\kappa-1)), \\ \Delta^{\iota}\mathscr{Y}(\mathtt{a}) = \mathscr{Y}_{\iota}, \quad \iota = 0, ..., \mathtt{m}-1, \end{cases} $$

where $\mathtt{m} = \lceil\kappa\rceil + 1$, is expressed by:

$$ \mathscr{Y}(\mathtt{t}) = \mathscr{Y}_0(\mathtt{t}) + \frac{1}{\Gamma(\kappa)} \sum_{\mathtt{b}=\mathtt{a}+\mathtt{m}-\kappa}^{\mathtt{t}-\kappa} (\mathtt{t}-\mathtt{b}-1)^{\kappa-1}\mathscr{X}(\mathtt{b}+\kappa-1, \mathscr{Y}(\mathtt{b}+\kappa-1)), $$

with $\mathscr{Y}_0(\mathtt{t}) = \sum_{\iota=0}^{\mathtt{m}-1} \frac{(\mathtt{t}-\mathtt{a})^{\iota}}{\Gamma(\iota+1)}\Delta^{\iota}\mathscr{Y}(\mathtt{a})$.

Theorem 2. *[35] To analyze the stability of the zero equilibrium, consider the discrete commensurate system:*

$$ {}^{\mathtt{c}}\Delta_{\mathtt{a}}^{\kappa}\mathtt{g}(\mathtt{t}) = \mathscr{A}\mathtt{g}(\mathtt{t}+\kappa-1), \quad \mathtt{t} \in \mathbb{N}_{\mathtt{a}+1-\kappa}, \quad \mathscr{A} \in \mathbb{R}^{m\times m}, $$

where $\mathtt{g}(\mathtt{t}) = (\mathtt{g}_1(\mathtt{t}), ..., \mathtt{g}_{\mathtt{m}}(\mathtt{t}))^T$ is the state vector, $0 < \kappa \leq 1$. The zero solution is asymptotically stable if all eigenvalues $\lambda_{\mathtt{j}}$ of the matrix $\mathscr{A}$ satisfy:

$$ \lambda_{\mathtt{j}} \in \left\{ \upsilon \in \mathbb{C} : |\upsilon| < \left(2\cos\frac{|\arg\upsilon| - \pi}{2-\kappa}\right)^{\kappa} \quad \textit{and} \quad |\arg\upsilon| > \frac{\kappa\pi}{2} \right\}, \quad \mathtt{j} = 1, 2, ..., \mathtt{m}. \tag{2.1} $$

2.2. Fractional-order discrete computer virus model

To represent the spread of internet viruses, we develop a fractional discrete model, classifying computers by their connection status: Internal (connected) or external (disconnected), assuming all are initially connected. The first version of the SLB model was originally proposed by Yang et al. in [36] as follows:

$$\begin{cases} \dot{S} = \sigma - \mu S(L+B) + \alpha_1 L + \alpha_2 B - \sigma S, \\ \dot{L} = \mu S(L+B) - \alpha_1 L - \eta L - \sigma L, \\ \dot{B} = \eta L - \alpha_2 B - \sigma B, \end{cases} \tag{2.2}$$

where S is the percentage of computers without the virus, L is the percentage of computers that have the virus but it is hidden, and B is the percentage of computers actively spreading the virus. μ represents the network connection rate for computers. η is the breakout rate for latent infections. α_1 specifies the recovery rate of inactively infected computers. α_2 is the rate at which an infected computer restores its normal operation. σ signifies the external internet connection rate. It is assumed that the parameters are positive and $S(t) + L(t) + B(t) \equiv 1$.

Recognizing the computational benefits of discrete representations, we utilize difference equations to simplify the model (2.2), providing a discrete version of the continuous system

$$\begin{cases} S_{n+1} = S_n + h[\sigma - \mu S_n(L_n + B_n) + \alpha_1 L_n + \alpha_2 B_n - \sigma S_n], \\ L_{n+1} = L_n + h[\mu S_n(L_n + B_n) - \alpha_1 L_n - \eta L_n - \sigma L_n], \\ B_{n+1} = B_n + h[\eta L_n - \alpha_2 B_n - \sigma B_n]. \end{cases} \tag{2.3}$$

Using the first difference order form, the system (2.3) may be rewritten as:

$$\begin{cases} \Delta S = h[\sigma - \mu S_n(L_n + B_n) + \alpha_1 L_n + \alpha_2 B_n - \sigma S_n], \\ \Delta L = h[\mu S_n(L_n + B_n) - \alpha_1 L_n - \eta L_n - \sigma L_n], \\ \Delta B = h[\eta L_n - \alpha_2 B_n - \sigma B_n]. \end{cases} \tag{2.4}$$

Fractional-order calculus enables the modeling of systems with memory, where past states influence the present dynamics. In this context, the fractional form of the model in Eq (2.4) is introduced to more precisely capture these memory effects, which are essential for understanding the system's behavior. In the following analysis, we assume $h = 1$, which corresponds to a unit step size. This simplifies the formulation without loss of generality and is commonly adopted in discrete-time modeling.

$$\begin{cases} {}^{c}\Delta_{a}^{\kappa} S(t) &= \sigma - \mu S(t+\kappa-1)(L(t+\kappa-1) + B(t+\kappa-1)) + \alpha_1 L(t+\kappa-1) \\ &\quad +\alpha_2 B(t+\kappa-1) - \sigma S(t+\kappa-1), \\ {}^{c}\Delta_{a}^{\kappa} L(t) &= \mu S(t+\kappa-1)(L(t+\kappa-1) + B(t+\kappa-1)) - \alpha_1 L(t+\kappa-1) \\ &\quad -\eta L(t+\kappa-1) - \sigma L(t+\kappa-1), \\ {}^{c}\Delta_{a}^{\kappa} B(t) &= \eta L(t+\kappa-1) - \alpha_2 B(t+\kappa-1) - \sigma B(t+\kappa-1), \end{cases} \tag{2.5}$$

where ${}^{c}\Delta_{a}^{\kappa}$ is the fractional Caputo difference operator of order $0 < \kappa \leq 1$.

We apply discrete fractional calculus to model a computer virus, demonstrating its effectiveness in capturing system dynamics. Notably, altering the fractional order enhances complexity and can induce chaotic behavior.

3. Stability analysis of the fixed points

Using the reproduction number, we probe the local asymptotic stability of the equilibrium points in the fractional discrete computer virus model. To determine the fixed points of (2.5), we put: ${}^{\mathtt{c}}\Delta_{\mathtt{a}}^{\kappa}S(\mathtt{t}) = 0$, ${}^{\mathtt{c}}\Delta_{\mathtt{a}}^{\kappa}L(\mathtt{t}) = 0$ and ${}^{\mathtt{c}}\Delta_{\mathtt{a}}^{\kappa}B(\mathtt{t}) = 0$, which implies:

$$\begin{cases} \sigma - \mu S(L+B) + \alpha_1 L + \alpha_2 B - \sigma S = 0, \\ \mu S(L+B) - \alpha_1 L - \eta L - \sigma L = 0, \\ \eta L - \alpha_2 B - \sigma B = 0. \end{cases} \tag{3.1}$$

For $L = 0$ and $B = 0$, the system possesses a fixed point without infection $E_0 = (1, 0, 0)$, if $L \neq 0$ and $B \neq 0$, then the viral fixed point is $E^* = (S^*, L^*, B^*)$ such that,

$$B^* = \frac{\eta}{\alpha_2 + \sigma} L^*.$$

Substituting this into the second equation of (3.1), we get:

$$S^* = \frac{(\alpha_1 + \eta + \sigma)(\alpha_2 + \sigma)}{\mu(\alpha_2 + \eta + \sigma)}.$$

Next, by replacing the expressions for B^* and S^* in the first equation of (3.4), we obtain:

$$L^* = \frac{\alpha_2 + \sigma}{\alpha_2 + \eta + \sigma} \left(\frac{(\alpha_1 + \eta + \sigma)(\alpha_2 + \sigma)}{\mu(\alpha_2 + \eta + \sigma)} - 1 \right).$$

To ensure that L^* remains positive, the following condition must be satisfied $\frac{(\alpha_1+\eta+\sigma)(\alpha_2+\sigma)}{\mu(\alpha_2+\eta+\sigma)} > 1$.

The number of new computers, on average, that get infected from one infected computer over the course of its life cycle is known as the basal reproductive rate of the virus propagation model. As explained in [36], R_0 is given by:

$$R_0 = \frac{\mu}{\alpha_1 + \eta + \sigma} \left(1 + \frac{\eta}{\alpha_2 + \sigma} \right) = \frac{\mu(\alpha_2 + \eta + \sigma)}{(\alpha_1 + \eta + \sigma)(\alpha_2 + \sigma)}. \tag{3.2}$$

3.1. The virus-free fixed point

Here, we examine the local asymptotic stability of the infection-free equilibrium. We introduce the following variable transformation, putting $\rho = \mathtt{t} + \kappa - 1$,

$$\begin{cases} x_{11}(\rho) = S(\rho) - S_0 = S(\rho) - 1, \\ x_{12}(\rho) = L(\rho) - L_0 = L(\rho), \\ x_{13}(\rho) = B(\rho) - B_0 = B(\rho). \end{cases} \tag{3.3}$$

A new map with zero fixed point $(0, 0, 0)$ is obtained:

$$\begin{cases} {}^{\mathtt{c}}\Delta_{\mathtt{a}}^{\kappa}(x_{11}(\mathtt{t}) + S_0) & = \sigma - \mu(x_{11}(\rho) + 1)(x_{12}(\rho) + x_{13}(\rho)) \\ & \quad + \alpha_1 x_{12}(\rho) + \alpha_2 x_{13}(\rho) - \sigma(x_{11}(\rho) + 1), \\ {}^{\mathtt{c}}\Delta_{\mathtt{a}}^{\kappa}(x_{12}(\mathtt{t}) + L_0) & = \mu(x_{11}(\rho) + 1)(x_{12}(\rho) + x_{13}(\rho)) \\ & \quad - \alpha_1 x_{12}(\rho) - \eta x_{12}(\rho) - \sigma x_{12}(\rho), \\ {}^{\mathtt{c}}\Delta_{\mathtt{a}}^{\kappa}(x_{13}(\mathtt{t}) + B_0) & = \eta x_{12}(\rho) - \alpha_2 x_{13}(\rho) - \sigma x_{13}(\rho). \end{cases} \tag{3.4}$$

Proposition 1. *The system* (2.5) *has a locally asymptotically stable virus-free equilibrium* E_0 *if either the condition in equation* (3.5) *or that in equation* (3.6) *is satisfied.*

$$\sigma < 2^{\kappa}, \;\; A^2 \geq 4B, \;\; R_0 < 1, \;\; |\frac{-A \pm \sqrt{A^2 - 4B}}{2}| < 2^{\kappa}, \tag{3.5}$$

$$\sigma < 2^{\kappa}, \;\; A^2 < 4B, \;\; |\lambda_{2,3}| < \left(2\cos\frac{|\arg\lambda_{2,3}| - \pi}{2-\kappa}\right)^{\kappa}, \;\; |\arg\lambda_{2,3}| > \frac{\kappa\pi}{2}, \tag{3.6}$$

where $A = \frac{(\alpha_2+\sigma)(\alpha_1+\eta+\sigma)}{\alpha_2+\eta+\sigma}\left(\frac{\eta}{\alpha_2+\sigma} + \frac{\alpha_2+\eta+\sigma}{\alpha_1+\eta+\sigma} + 1 - R_0\right)$, $B = (\alpha_2+\sigma)(\alpha_1+\eta+\sigma)(1-R_0)$, and $\lambda_{2,3} = \frac{-A\pm\sqrt{A^2-4B}}{2}$.

Proof. We construct the Jacobian matrix associated with the model as follows in order to see if the virus-free fixed point stays steady.

$$J = \begin{pmatrix} -\mu h(x_{12}+x_{13}) - \sigma h & -\mu h(x_{11}+1) + \alpha_1 h & -\mu h(x_{11}+1) + \alpha_2 h \\ \mu h(x_{12}+x_{13}) & \mu h(x_{11}+1) - (\alpha_1+\eta+\sigma)h & \mu h(x_{11}+1) \\ 0 & \eta h & -(\alpha_2+\sigma)h \end{pmatrix}.$$

By simple calculation we put h=1, we obtain the jacobian matrix of the free fixed point

$$J_0 = \begin{pmatrix} -\sigma & -\mu+\alpha_1 & -\mu+\alpha_2 \\ 0 & \mu-(\alpha_1+\eta+\sigma) & \mu \\ 0 & \eta & -(\alpha_2+\sigma) \end{pmatrix}, \tag{3.7}$$

the corresponding characteristic equation:

$$(-\sigma-\lambda)(\lambda^2 + A\lambda + B) = 0, \tag{3.8}$$

where

$$A = \frac{(\alpha_2+\sigma)(\alpha_1+\eta+\sigma)}{\alpha_2+\eta+\sigma}\left(1 + \frac{\eta}{\alpha_2+\sigma} + \frac{\alpha_2+\eta+\sigma}{\alpha_1+\eta+\sigma} - R_0\right),$$
$$B = (\alpha_2+\sigma)(\alpha_1+\eta+\sigma)(1-R_0).$$

The eigenvalues of J_0 are $\lambda_1 = -\sigma$, $\lambda_{2,3} = \frac{-A\pm\sqrt{A^2-4B}}{2}$,
hence,

$$|\arg\lambda_1| = \pi > \frac{\kappa\pi}{2},$$

the condition $|\lambda_1| < \left(2\cos\frac{|\arg\lambda_1|-\pi}{2-\kappa}\right)^{\kappa} = 2^{\kappa}$ is satisfied if $\sigma < 2^{\kappa}$.

For $\lambda_{2,3}$ if $R_0 < 1$, we get $A > 0$ and $B > 0$, by the Routh-Hurwitz criterion, (a detailed treatment of this criterion and its application in mathematical modeling can be found in [37]. We are able to conclude that the roots of Eq (3.8) are in the left half plane, for $A^2 - 4B > 0$, and the eigenvalues $\lambda_{2,3}$ arguments are π, therefore,

$$|\arg\lambda_{2,3}| = \pi > \frac{\kappa\pi}{2},$$

the condition $|\lambda_{2,3}| < \left(2\cos\frac{|\arg\lambda_{2,3}|-\pi}{2-\kappa}\right)^{\kappa} = 2^{\kappa}$ is satisfied if $|\frac{-A\pm\sqrt{A^2-4B}}{2}| < 2^{\kappa}$.

In the case where $A^2 - 4B = 0$, the characteristic roots are given by

$$\lambda_{2,3} = \frac{-A}{2},$$

since $R_0 < 1$ implies $A > 0$, we have $\lambda_{2,3} < 0$. Therefore, $|\arg(\lambda_{2,3})| = \pi$. As a result, the condition $|\arg(\lambda_{2,3})| > \frac{\kappa\pi}{2}$ is automatically satisfied for all $0 < \kappa \leq 1$.

Now, when $A^2 < 4B$, we find that the eigenvalues $\lambda_{2,3}$ are complex, and the stability is verified if

$$|\lambda_{2,3}| < \left(2\cos\frac{|\arg\lambda_{2,3}| - \pi}{2 - \kappa}\right)^{\kappa} \text{ and } |\arg\lambda_{2,3}| > \frac{\kappa\pi}{2}. \tag{3.9}$$

Therefore, since the condition in Theorem 2 is satisfied, the virus-free equilibrium E_0 of system (2.5) is locally asymptotically stable. □

3.2. The Viral fixed point

In this subsection, we investigate the local asymptotic stability of the viral equilibrium in the framework of the proposed computer virus model. The viral fixed point is given by $E^* = (S^*, L^*, B^*)$ such as:

$$S^* = \frac{1}{R_0} = \frac{(\alpha_1 + \eta + \sigma)(\alpha_2 + \sigma)}{\mu(\alpha_2 + \eta + \sigma)}, \tag{3.10}$$

$$L^* = \frac{(1 - \frac{1}{R_0})(\alpha_2 + \sigma)}{\alpha_2 + \eta + \sigma} = \frac{(R_0 - 1)(\alpha_2 + \sigma)}{R_0(\alpha_2 + \eta + \sigma)}, \tag{3.11}$$

$$B^* = \frac{\eta(1 - \frac{1}{R_0})}{\alpha_2 + \eta + \sigma} = \frac{\eta(R_0 - 1)}{R_0(\alpha_2 + \eta + \sigma)}. \tag{3.12}$$

Note that if $R_0 < 1$, the system admits just a virus-free equilibrium point E_0.

With the same manner and via a direct calculation, we find the jacobian matrix of the viral fixed point.

$$J^* = \begin{pmatrix} -\mu(L^* + B^*) - \sigma & -\mu S^* + \alpha_1 & -\mu S^* + \alpha_2 \\ \mu(L^* + B^*) & \mu S^* - (\alpha_1 + \eta + \sigma) & \mu S^* \\ 0 & \eta & -(\alpha_2 + \sigma) \end{pmatrix}, \tag{3.13}$$

the corresponding characteristic equation:

$$\lambda^3 + A_1\lambda^2 + B_1\lambda + C_1 = 0, \tag{3.14}$$

where

$$\begin{cases} A_1 & = \mu\left(1 - \frac{2}{R_0}\right) + 3\sigma + \alpha_1 + \alpha_2 + \eta, \\ B_1 & = \left[\mu\left(1 - \frac{1}{R_0}\right) + \sigma\right]\left[\alpha_1 + \eta + \sigma - \frac{\mu}{R_0}\right] + \mu\left(1 - \frac{1}{R_0}\right)\left(\frac{\mu}{R_0} - \alpha_2\right) \\ & \quad +\eta\left(\frac{\mu}{R_0} - \alpha_1\right) - (\alpha_2 + \sigma)\left[\mu\left(1 - \frac{1}{R_0}\right) + \sigma\right] - (\alpha_2 + \sigma)\left(\frac{\mu}{R_0} - \alpha_1 - \eta - \sigma\right), \\ C_1 & = \left[\mu\left(1 - \frac{1}{R_0}\right) + \sigma\right]\left(\frac{\mu}{R_0} - \alpha_1 - \eta - \sigma\right)(\alpha_2 + \sigma) \\ & \quad -\mu\left(1 - \frac{1}{R_0}\right)\left(-\frac{\mu}{R_0} + \alpha_2\right)\eta + \mu\left(1 - \frac{1}{R_0}\right)\frac{\mu}{R_0}(\alpha_2 + \sigma). \end{cases}$$

Accordingly, the stability characteristics of the viral fixed point within the fractional discrete computer virus model are evaluated numerically, based on the formula (2.1).

To validate the analytical results and explore the dynamical behavior of the fractional-order system, we perform numerical simulations under different parameter settings. In each case, the values are chosen to reflect meaningful scenarios in terms of infection spread, recovery, and system connectivity. These simulations aim to illustrate the system's behavior in three regimes: Virus-free stability, viral equilibrium stability, and chaotic dynamics.

Example 1. Using parameters $\eta = 0.6, \mu = 0.3, \sigma = 0.1, \alpha_1 = 0.1$, and $\alpha_2 = 0.3$, which imply $R_0 = 0.9375$, so $R_0 < 1$. The time series of S, L, and B exhibited in Figure 1(a), demonstrates the asymptotic stability of the virus-free fixed points.

Example 2. Using parameters $\eta = 0.6, \mu = 0.4, \sigma = 0.1, \alpha_1 = 0.1$, and $\alpha_2 = 0.3$, which imply $R_0 = 1.25$, we get $R_0 > 1$. The time series of S, L, and B exhibited in Figure 1(b), demonstrates the asymptotic stability of the viral equilibrium.

Example 3. Using parameters $\eta = 2, \mu = 2, \sigma = 0.1, \alpha_1 = 0.1$, and $\alpha_2 = 0.3$, the time series of S, L, and B exhibited in Figure 1(c), demonstrates the instability of the fixed points. Therefore, the fractional model (2.5) meets the necessary conditions for the occurrence of chaos.

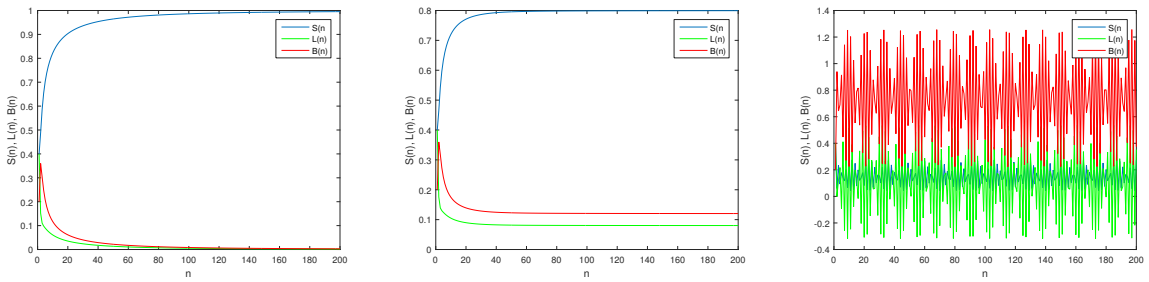

(a) **(b)** **(c)**

Figure 1. The trajectories of change of S, L, and B with $\kappa = 0.98$: (a) for $\eta = 0.6, \mu = 0.3, \sigma = 0.1, \alpha_1 = 0.1$, and $\alpha_2 = 0.3$; (b) for $\eta = 0.6, \mu = 0.4, \sigma = 0.1, \alpha_1 = 0.1$, and $\alpha_2 = 0.3$; (c) for $\eta = 2, \mu = 2, \sigma = 0.1, \alpha_1 = 0.1$, and $\alpha_2 = 0.3$.

In general, as the fractional-order parameter κ decreases, the system experiences stronger memory effects, which slow down the virus spread, resulting in a lower R_0. Conversely, as κ approaches 1, the memory effects diminish, causing the system to behave more like a traditional model, which leads to an increase in R_0.

4. Nonlinear dynamics of the fractional-order discrete computer virus model

We explore how the fractional model in commensurate order behaves chaotically. This analysis includes visualizing bifurcation and phase portraits, as well as calculating the maximum Lyapunov exponent. To understand the model's features, we also supply the numerical formulation, resulting from Theorem 1, used for simulations

$$\begin{cases} S(\mathtt{n}) = S(0) + \frac{1}{\Gamma(\kappa)} \sum_{\mathtt{j}=1}^{\mathtt{n}} \frac{\Gamma(\mathtt{n}-\mathtt{j}+\kappa)}{\Gamma(\mathtt{n}-\mathtt{j}+1)} & [\sigma - \mu S(\mathtt{j}-1)(L(\mathtt{j}-1) + B(\mathtt{j}-1)) \\ & +\alpha_1 L(\mathtt{j}-1) + \alpha_2 B(\mathtt{j}-1) - \sigma S(\mathtt{j}-1)], \\ L(\mathtt{n}) = L(0) + \frac{1}{\Gamma(\kappa)} \sum_{\mathtt{j}=1}^{\mathtt{n}} \frac{\Gamma(\mathtt{n}-\mathtt{j}+\kappa)}{\Gamma(\mathtt{n}-\mathtt{j}+1)} & [\mu S(\mathtt{j}-1)(L(\mathtt{j}-1) + B(\mathtt{j}-1)) \\ & -\alpha_1 L(\mathtt{j}-1) - \eta L(\mathtt{j}-1) - \sigma L(\mathtt{j}-1)], \\ B(\mathtt{n}) = B(0) + \frac{1}{\Gamma(\kappa)} \sum_{\mathtt{j}=1}^{\mathtt{n}} \frac{\Gamma(\mathtt{n}-\mathtt{j}+\kappa)}{\Gamma(\mathtt{n}-\mathtt{j}+1)} & [\eta L(\mathtt{j}-1) - \alpha_2 B(\mathtt{j}-1) - \sigma B(\mathtt{j}-1)], \end{cases} \tag{4.1}$$

where $S(0)$, $L(0)$, and $B(0)$ are the initial conditions. Lyapunov exponents are closely tied to bifurcation analysis and are crucial for identifying unpredictable behavior in fractional maps. In [38], a valuation of the Lyapunov exponents for the fractional system was conducted by the authors via the Jacobian matrix approach. This method effectively captures the chaotic dynamics that are characteristic of fractional-order maps. A key component of this analysis is the tangent map, which integrates discrete memory effects, and occurs because the system's behavior depends not solely on its present condition but also on its past states. The tangent map is expressed as follows:

$$J_n = \begin{pmatrix} a_1(n) & a_2(n) & a_3(n) \\ b_1(n) & b_2(n) & b_3(n) \\ d_1(n) & d_2(n) & d_3(n) \end{pmatrix}, \tag{4.2}$$

such that

$$\begin{cases} a_\iota(n) = a_\iota(0) + \frac{1}{\Gamma(\kappa)} \sum_{j=1}^{n} \frac{\Gamma(n-j+\kappa)}{\Gamma(n-j+1)} & ((-\sigma - \mu(L(j-1) + B(j-1)))a_\iota(j-1) \\ & +(\alpha_1 - \mu S(j-1))b_\iota(j-1) + (\alpha_2 - \mu S(j-1))d_\iota(j-1)), \\ b_\iota(n) = b_\iota(0) + \frac{1}{\Gamma(\kappa)} \sum_{j=1}^{n} \frac{\Gamma(n-j+\kappa)}{\Gamma(n-j+1)} & (\mu(L(j-1) + B(j-1))a_\iota(j-1) \\ & +(\mu S(j-1) - \alpha_1 - \eta - \sigma)b_\iota(j-1) + \mu S(j-1)d_\iota(j-1)), \\ d_\iota(n) = d_\iota(0) + \frac{1}{\Gamma(\kappa)} \sum_{j=1}^{n} \frac{\Gamma(n-j+\kappa)}{\Gamma(n-j+1)} & (\eta b_\iota(j-1) - (\alpha_2 + \sigma)d_\iota(j-1)), \end{cases} \tag{4.3}$$

using the identity matrix as initial conditions

$$\begin{pmatrix} a_1(0) & a_2(0) & a_3(0) \\ b_1(0) & b_2(0) & b_3(0) \\ d_1(0) & d_2(0) & d_3(0) \end{pmatrix} = \begin{pmatrix} 1 & 0 & 0 \\ 0 & 1 & 0 \\ 0 & 0 & 1 \end{pmatrix}. \tag{4.4}$$

Then, the Lyapunov exponents are defined by:

$$LE_\ell = \lim_{n\to\infty} \frac{1}{n} \ln |\lambda_\ell^{(n)}|, \quad for \ \ \ell = 1, 2, 3, \tag{4.5}$$

where λ_ℓ ($\ell = 1, 2, 3$) are the eigenvalues of J_n.

For a detailed look at the characteristics and behavior of (2.5), see Figure 2, which shows bifurcation diagrams of (2.5) as a dependence on the parameter η with variations in κ, illustrating the system's dynamical behavior starting from $(0.4, 0.4, 0.2)$. In subfigures (a) and (b), where $\mu = 2.2, \sigma = 0.06, \alpha_1 = 0.05, \alpha_2 = 1$, and $\kappa = 0.98$ and $\kappa = 0.95$, the diagrams reveal a widespread scattering of points, indicating persistent chaotic dynamics. The dense and seemingly random distribution of points suggests that even small changes in η significantly alter the system's trajectory. The extensive

presence of chaos across a broad range of η values highlights the system's high instability. In subfigures (c) and (d), which also correspond to $\kappa = 0.98$ and $\kappa = 0.95$ but with different parameters $\mu = 2.1, \sigma = 0.1, \alpha_1 = 0.1$, and $\alpha_2 = 0.3$, a structured transition from periodic to chaotic behavior is observed. Initially, periodic orbits are visible, but as η increases, period-doubling bifurcations drive the system into chaotic states. Periodic windows within chaotic regions indicate intermittent stabilization, showcasing the system's complex dynamics. Figure 3 depicts the variation of the Maximum Lyapunov Exponent (MLE) with respect to η, providing a quantitative measure of the system's stability. In subfigures (a) and (b), where $\kappa = 0.98$, and $\kappa = 0.95$, the MLE remains consistently positive, confirming chaotic behavior. A positive MLE signifies exponential divergence of nearby trajectories, reflecting strong instability. In subfigures (c) and (d), which correlate with different parameters but the same κ values, the MLE demonstrates a sign-changing fluctuation. This fluctuation indicates shifts between periodic and chaotic states, with negative MLE values corresponding to periodic stability and positive values confirming chaotic behavior. These results further emphasize the system's susceptibility to parameter variations.

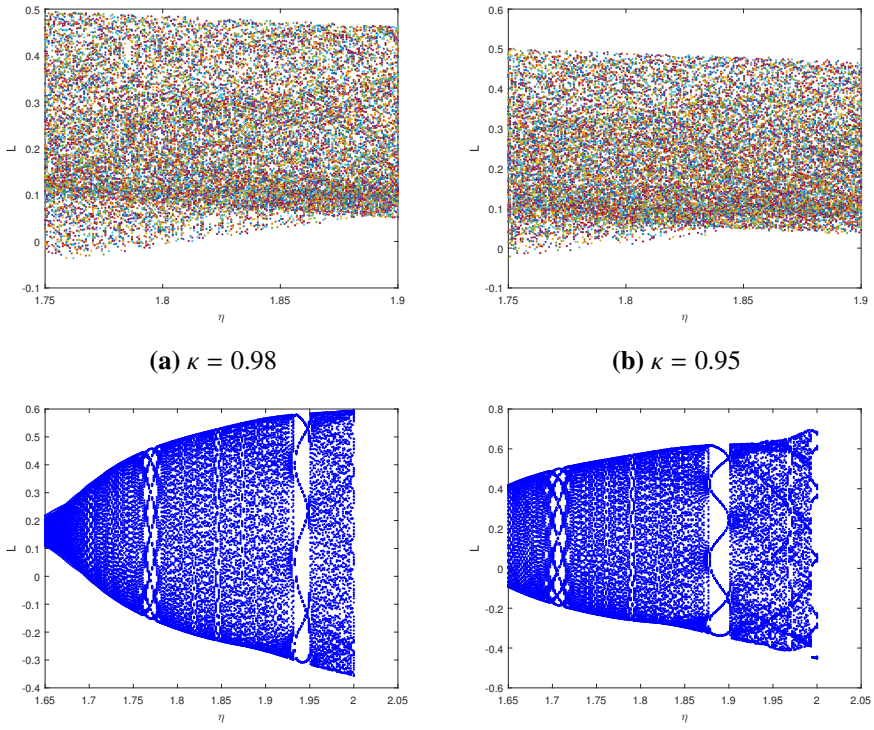

(a) $\kappa = 0.98$ **(b)** $\kappa = 0.95$

(c) $\kappa = 0.98$ **(d)** $\kappa = 0.95$

Figure 2. Bifurcation diagram of (2.5) versus η for differing κ values with IC=$(0.4, 0.4, 0.2)$: (a), (b) for $\mu = 2.2, \sigma = 0.06, \alpha_1 = 0.05$, and $\alpha_2 = 1$; (c), (d) for $\mu = 2.1, \sigma = 0.1, \alpha_1 = 0.1$, and $\alpha_2 = 0.3$.

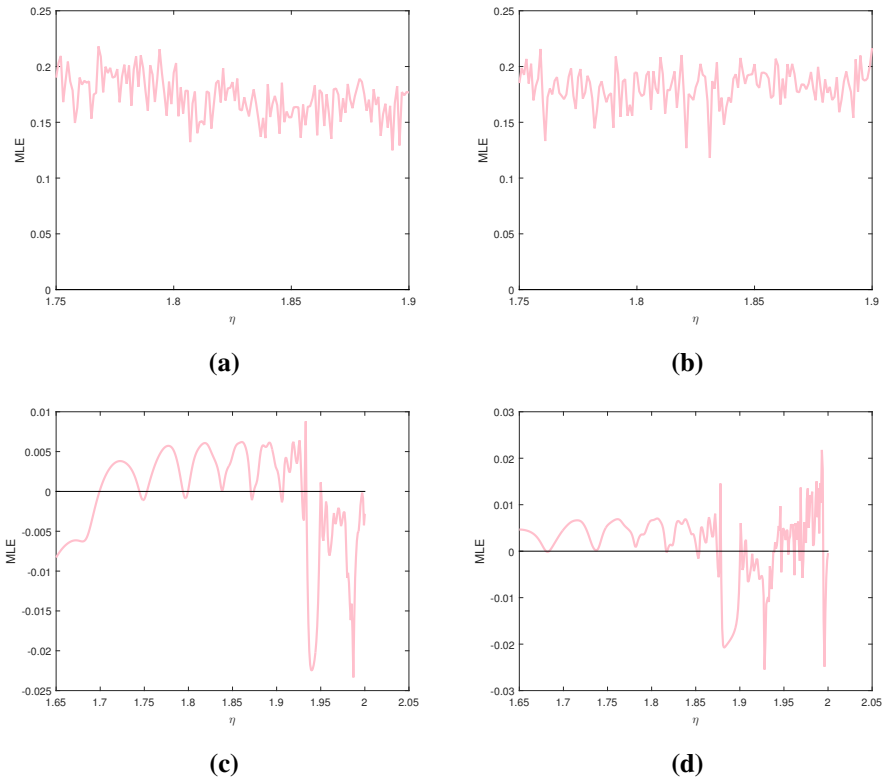

Figure 3. MLE of (2.5) versus η for differing κ values with IC=$(0.4, 0.4, 0.2)$: (a), (b) for $\mu = 2.2, \sigma = 0.06, \alpha_1 = 0.05$, and $\alpha_2 = 1$; (c), (d) for $\mu = 2.1, \sigma = 0.1, \alpha_1 = 0.1$, and $\alpha_2 = 0.3$.

The influence of α_2 relating to the system's time-dependent behavior is visualized in Figure 4 using bifurcation diagrams. Setting the initial conditions to $(0.4, 0.4, 0.2)$, subfigures 4(a) and 4(b), where $\kappa = 0.98$ and $\kappa = 0.95$, the diagrams show a passage from periodic to chaotic attractors as α_2 increases. Period-doubling cascades signify a gradual shift toward chaos, with periodic windows indicating temporary stabilization. In Figures 4(c) and 4(d), with distinct parameter settings, but identical κ values, the system retains periodicity over a wider range of α_2 before transitioning to chaos. This transition, being less abrupt than in 4(a) and 4(b), indicates a longer duration of stability and reinforces the system's reliance on α_2. To quantify the system's stability through MLE analysis as a function of α_2, Figure 5 is shown. In 5 (a) and 5(b), the MLE increases with α_2, confirming a transition from periodic to chaotic behavior. Positive MLE values at higher α_2 indicate persistent chaos. In subfigures 5(c) and 5(d), under different parameterizations, while maintaining the same values κ, the MLE alternates between positive and negative values. This alternation reflects periodic and chaotic states, with periodic behavior dominating at lower α_2 and chaos prevailing at higher values. These findings further illustrate the system's complex and sensitive nature. This analysis reveals several key observations. Increasing η drives the system toward chaos, as evidenced by bifurcation diagrams and MLE plots. Similarly, increasing α_2 induces period-doubling bifurcations, producing chaotic states with intermittent periodic domains. The system also demonstrates strong sensitivity to κ, with both values (0.98 and 0.95) contributing to chaotic dynamics. These results underscore the system's complexity and its pronounced sensitivity to parameter variations, highlighting the intricate interplay

between periodic and chaotic regimes.

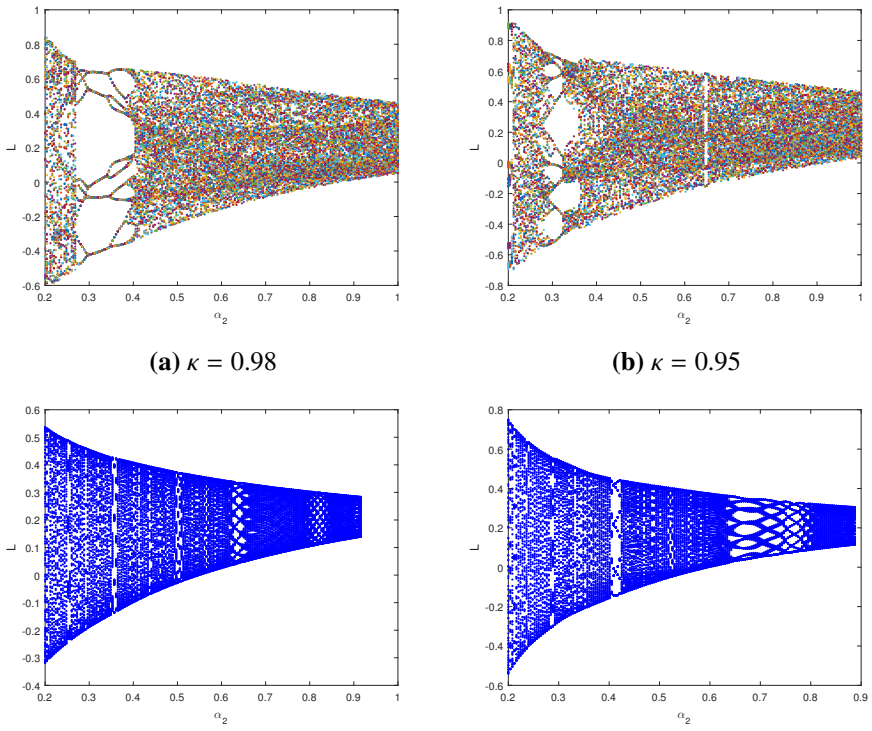

(a) $\kappa = 0.98$ **(b)** $\kappa = 0.95$

(c) $\kappa = 0.98$ **(d)** $\kappa = 0.95$

Figure 4. Bifurcation diagram versus α_2 of (2.5) for differing κ values with IC=(0.4, 0.4, 0.2); (a), (b) for $\eta = 1.9, \mu = 2.2, \sigma = 0.06$, and $\alpha_1 = 0.05$; (c), (d) for $\eta = 2, \mu = 2, \sigma = 0.1$, and $\alpha_1 = 0.1$.

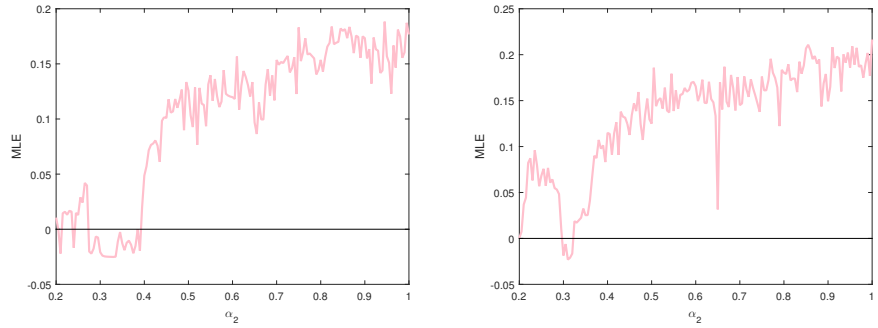

(a) $\kappa = 0.98$ **(b)** $\kappa = 0.95$

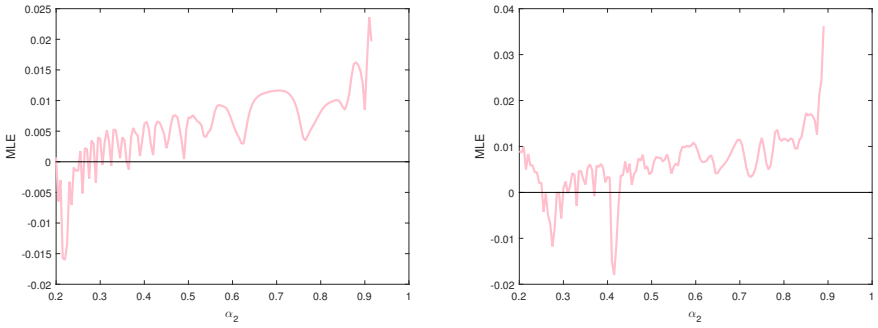

(c) $\kappa = 0.98$ **(d)** $\kappa = 0.95$

Figure 5. MLE versus α_2 of (2.5) for differing κ values with IC=$(0.4, 0.4, 0.2)$; (a), (b) for $\eta = 1.9, \mu = 2.2, \sigma = 0.06$, and $\alpha_1 = 0.05$; (c), (d) for $\eta = 2, \mu = 2, \sigma = 0.1$, and $\alpha_1 = 0.1$.

Now, we focus on the effect caused by the fractional-order parameter κ regarding the evolutionary patterns of the discrete fractional computer virus system. The bifurcation diagrams and the related MLE plots are illustrated in Figure 6. The left column, including (a), (c), and (e), displays the bifurcation diagrams, while the right column, which displays (b), (d), and (f), presents the MLE variations. In subfigure (a), corresponding to $\eta = 1.9, \mu = 2.1, \sigma = 0.1, \alpha_1 = 0.1$, and $\alpha_2 = 0.3$, the bifurcation diagram exhibits significant chaotic behavior, with a wide spread of trajectories over the κ range. The corresponding MLE in (b) confirms this, as it remains predominantly positive, indicating strong chaos. Subfigures (c) and (d), for $\eta = 2, \mu = 2, \sigma = 0.1, \alpha_1 = 0.1$, and $\alpha_2 = 0.3$, demonstrate a gradual transition from chaos to periodicity as κ increases, with the MLE plot showing a decline toward negative values. In subfigure (e), where $\eta = 1.9, \mu = 1.98, \sigma = 0.1, \alpha_1 = 0.1$, and $\alpha_2 = 0.3$, a mixed dynamic behavior is observed with intermittent chaos and periodic windows, as indicated by the fluctuating MLE in (f). Overall, the results suggest that the system's dynamics are highly sensitive to κ. While larger values of κ can sustain chaotic dynamics in some cases, in others, increasing κ may lead to a transition toward periodicity. The fractional order κ significantly affects the system's dynamics. Lower values of κ enhance memory effects, often leading to chaos, while increasing κ tends to stabilize the system, resulting in periodic or steady behavior. This transition highlights the key role of κ in controlling the system's evolution and the nuanced significance of the fractional exponent in governing the model's complexity and stability.

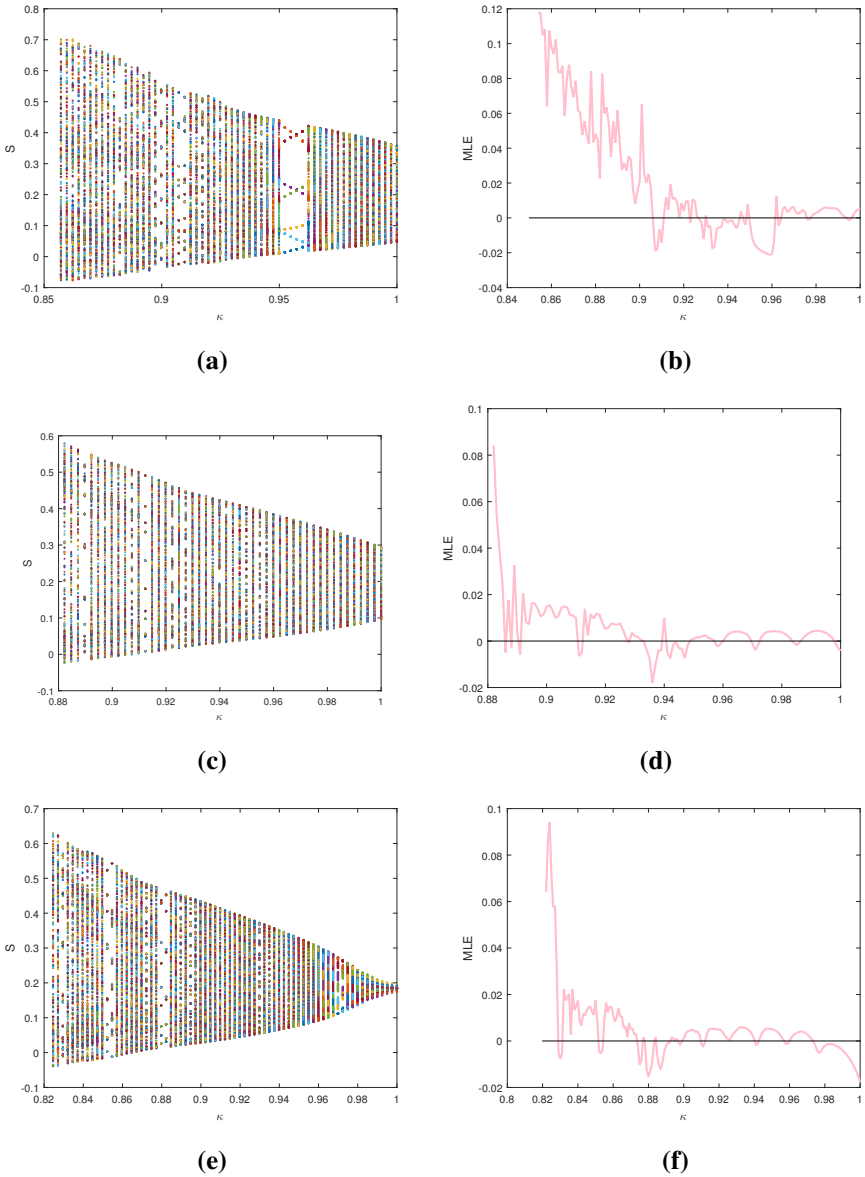

Figure 6. Bifurcation diagrams and the corresponding MLE of (2.5) versus the fractional-order κ with IC=$(0.4, 0.4, 0.2)$; (a), (b) for $\eta = 1.9, \mu = 2.1, \sigma = 0.1, \alpha_1 = 0.1$, and $\alpha_2 = 0.3$; (c), (d) for $\eta = 2, \mu = 2, \sigma = 0.1, \alpha_1 = 0.1$, and $\alpha_2 = 0.3$; (e), (f) for $\eta = 1.9, \mu = 1.98, \sigma = 0.1, \alpha_1 = 0.1$, and $\alpha_2 = 0.3$.

Moreover, Figure 7 shows case phase portraits changing the fractional parameter κ, specifically for $\kappa = 0.855, 0.856, 0.858, 0.859, 0.86, 0.88, 0.89$, and 0.9. These phase portraits visually represent the system's attractors under different fractional orders. Upon analysis of these portraits, we can identify the diverse dynamical feature manifests in the fractional discrete computer virus model. As κ increases, the system undergoes significant transitions in its dynamical behavior. At lower values of κ, the trajectories appear scattered and weakly structured, suggesting transient chaotic or irregular motion. As κ increases, more distinct attractors begin to form, signaling a shift toward stable periodic or chaotic motion. This evolution underscores the model's sensitivity to the alterations of the fractional-order

parameter, producing a broad array of dynamic behaviors. Virus propagation in real-world networks can exhibit chaotic behavior due to nonlinear feedback, randomness, and adaptive malware. This leads to unpredictable outbreaks and irregular infection patterns. Modeling such dynamics with chaos theory helps develop more adaptive and responsive defense strategies that react effectively to small changes in the threat environment.

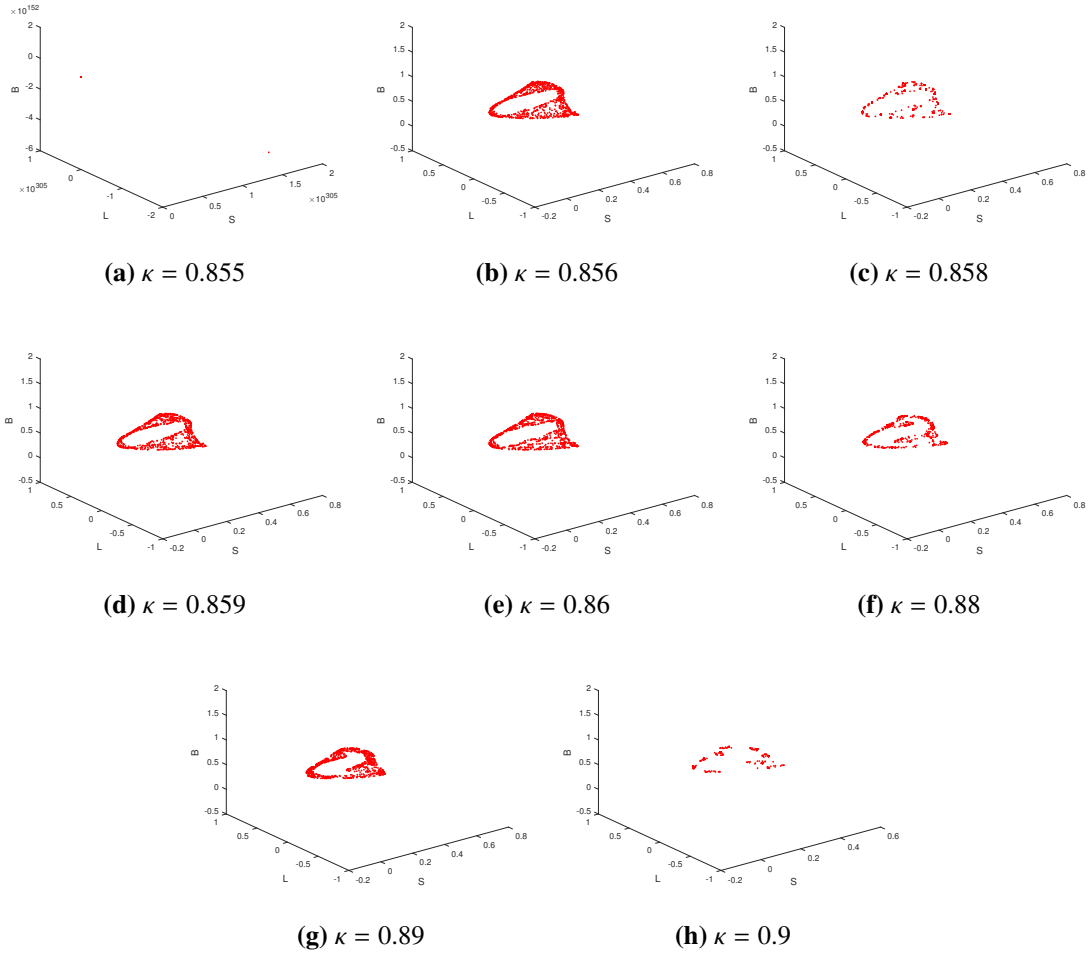

(a) $\kappa = 0.855$ **(b)** $\kappa = 0.856$ **(c)** $\kappa = 0.858$

(d) $\kappa = 0.859$ **(e)** $\kappa = 0.86$ **(f)** $\kappa = 0.88$

(g) $\kappa = 0.89$ **(h)** $\kappa = 0.9$

Figure 7. Trajectory plots of (2.5) with IC=(0.4, 0.4, 0.2) and $\eta = 1.9, \mu = 2.1, \sigma = 0.1, \alpha_1 = 0.1$, and $\alpha_2 = 0.3$, for differing κ values.

Figure 8 presents a bifurcation diagram and the corresponding MLE for the system of fractional order (2.5) as a parametric function of κ, using specific parameter values: $\eta = 1.2$, $\mu = 2.1$, $\sigma = 0.1$, $\alpha_1 = 0.1$, and $\alpha_2 = 0.6$. Figures 8(a), (b), and (c) show the bifurcation diagrams for S, L, and B, respectively. These diagrams reveal a transition from chaotic behavior at lower values of κ (approximately 0.4656 to 0.62) to a more stable, periodic, or fixed-point behavior at higher values of κ (approximately 0.9 to 1). This is evident from the scattered points at lower κ values, indicating complex and unpredictable dynamics, and the convergence to distinct lines or points at higher κ values, suggesting simpler, more regular behavior. Subfigure 8(d) shows the MLE as a function of κ. Consistent with the bifurcation diagrams, the MLE is positive at lower κ values, confirming the presence of chaotic behavior. As κ increases, the MLE decreases and becomes negative around

$\kappa \approx 0.63$, indicating a transition to a stable regime. This alignment between the bifurcation diagrams and the MLE plot reinforces the observation that the system transitions from chaos to stability as κ increases. Compared to the previous case, this parameter set exhibits a wider chaotic range. Also, we have generated the phase portrait, which is depicted in Figure 9. At low fractional order κ, trajectories show dense, chaotic behavior. As κ increases, the system transitions, with the attractor breaking into clusters, suggesting a shift towards periodicity or stability. Beyond $\kappa = 0.61$, the system becomes more scattered, indicating reduced chaos. In summary, these analyses reveal that the fractional discrete computer virus model exhibits multiple dynamical regimes, encompassing chaotic dynamics, periodic oscillations, and stable states, contingent on the value of κ. These insights enhance our grasp of fractional-order discrete systems and their intricate dynamics. We compare our fractional-order virus propagation model with existing integer-order SIR models and continuous-time fractional-order models. Unlike integer-order models, which lack memory effects, our model captures long-term memory and nonlinearity, providing a more accurate representation of virus dynamics. Additionally, our discrete-time approach offers greater flexibility for systems with discrete data, making it better suited for real-time simulations and virus tracking. This distinction is essential for modeling chaotic behavior and synchronization, which continuous-time models may not fully capture, thus enhancing the accuracy and applicability of our approach in cybersecurity.

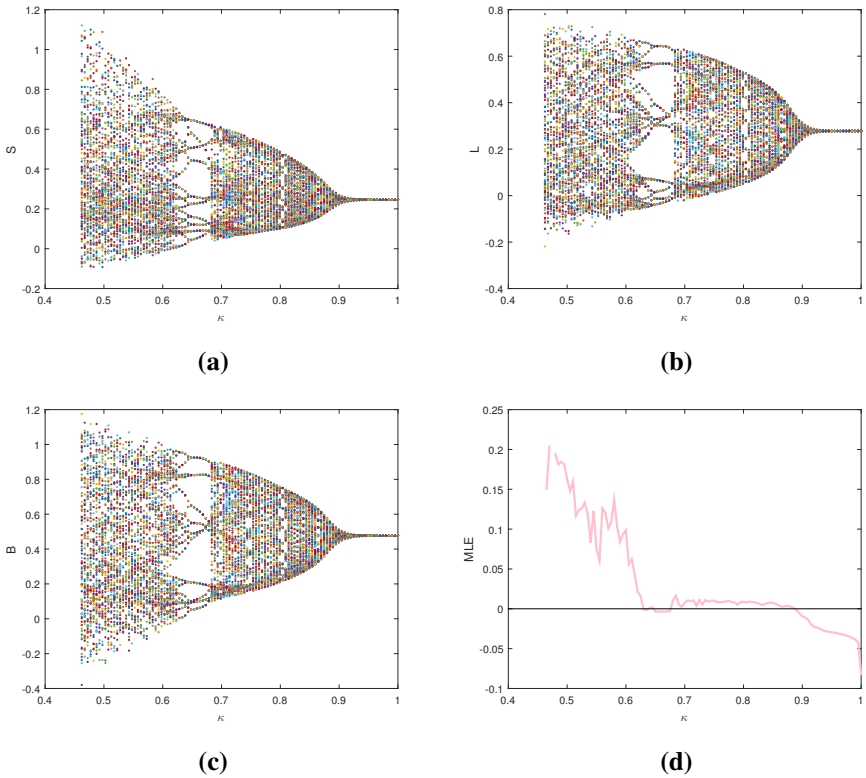

Figure 8. Bifurcation diagrams and the corresponding MLE of (2.5) versus κ, with IC=$(0.4, 0.4, 0.2)$ and $\eta = 1.2$, $\mu = 2.1$, $\sigma = 0.1$, $\alpha_1 = 0.1$, and $\alpha_2 = 0.6$.

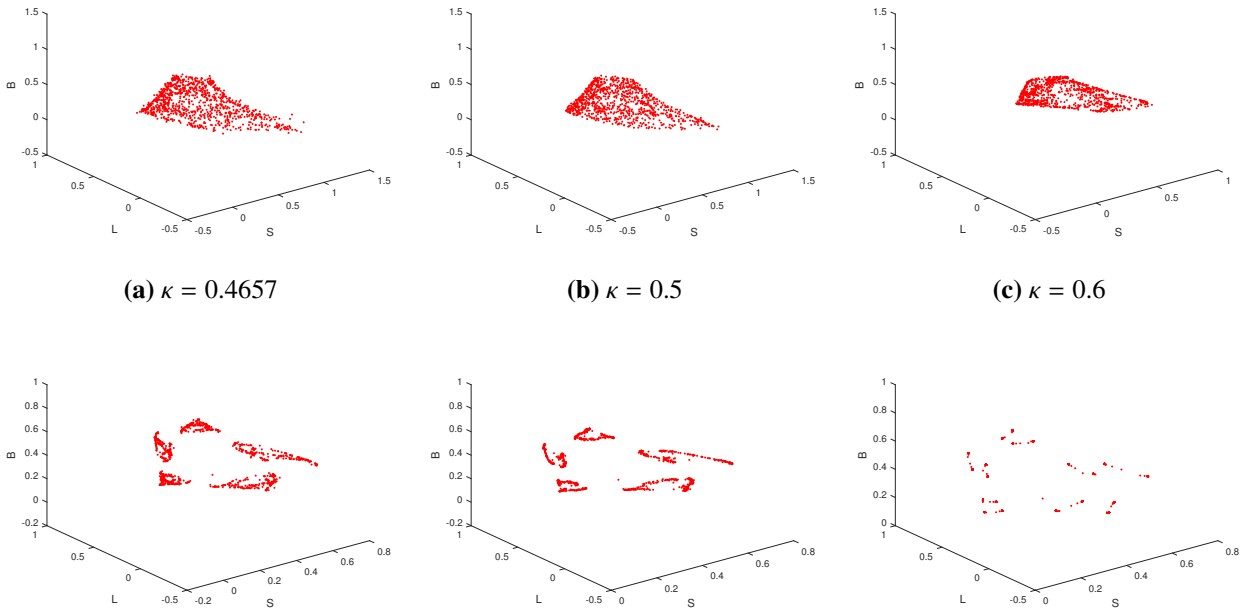

(a) $\kappa = 0.4657$ **(b)** $\kappa = 0.5$ **(c)** $\kappa = 0.6$

(d) $\kappa = 0.61$ **(e)** $\kappa = 0.62$ **(f)** $\kappa = 0.63$

Figure 9. Trajectory plots of (2.5) with IC=$(0.4, 0.4, 0.2)$ and $\eta = 1.2$, $\mu = 2.1$, $\sigma = 0.1$, $\alpha_1 = 0.1$, and $\alpha_2 = 0.6$ for differing κ values.

The fractional-order κ captures memory effects, influencing how past infections affect current dynamics. While not directly equivalent to propagation or recovery rates, κ modulates their impact over time. Mapping κ to real-world values would require data fitting or parameter estimation in future studies.

5. Approximate entropy, C_0 complexity, and permutation entropy

In this section, we employ complexity analysis to evaluate the unpredictability and irregularity of dynamical systems, focusing on the generated keystreams. Specifically, we utilize Approximate Entropy (ApEn) [39], the C_0 complexity algorithm [40], and Permutation Entropy (PE) [41], to assess their randomness and structural richness. ApEn quantifies pattern regularity and unpredictability, PE examines the temporal ordering of values, and C0 analyzes local fluctuations, thereby collectively offering a comprehensive characterization of the system's complexity.

The ApEn of (2.5) was analyzed for $\sigma = 0.1, \alpha_1 = 0.1$, and $\alpha_2 = 0.3$, with the results presented in Figure 10. The analysis reveals that the complexity of the model varies with changes in κ, with the utmost ApEn observed when the system exhibits chaotic behavior. This observation aligns well with the maximum Lyapunov exponent results. Therefore, careful selection of κ values in system (2.5) is crucial to achieving a relatively high structural complexity.

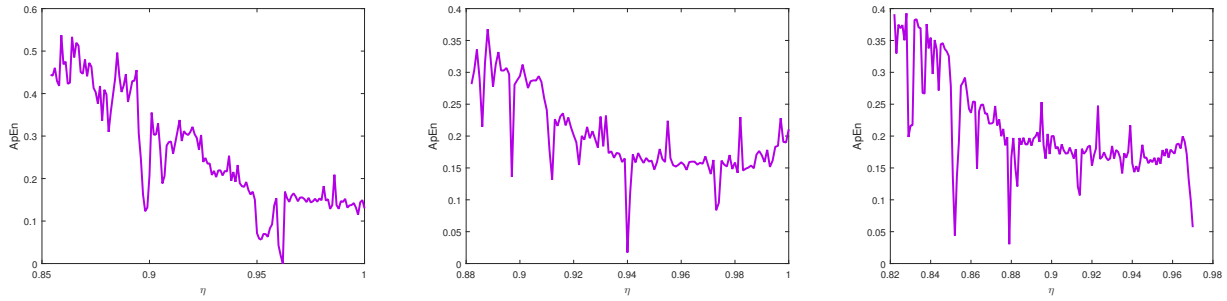

(a) **(b)** **(c)**

Figure 10. ApEn of (2.5) versus κ with IC=(0.4, 0.4, 0.2): for (a) $\eta = 1.9, \mu = 2.1$; (b) $\eta = 2, \mu = 2$; (c) $\eta = 1.9$, and $\mu = 1.98$.

Additionally, Figure 11 visually represents the C_0 Complexity analysis of the discrete fractional-order computer virus model (2.5), demonstrating its dynamics under varied parameter conditions $\sigma = 0.1, \alpha_1 = 0.1$, and $\alpha_2 = 0.3$. Figure 11(a) shows the configuration with $\eta = 1.9, \mu = 2.1$, and $\kappa \in [0.85, 1]$. Figure 11(b), on the other hand, illustrates the behavior when $\eta = 2, \mu = 2$, and $\kappa \in [0.88, 1]$ while Figure 11(c) corresponds to $\eta = 1.9, \mu = 1.98$, and $\kappa \in [0.82, 0.98]$.

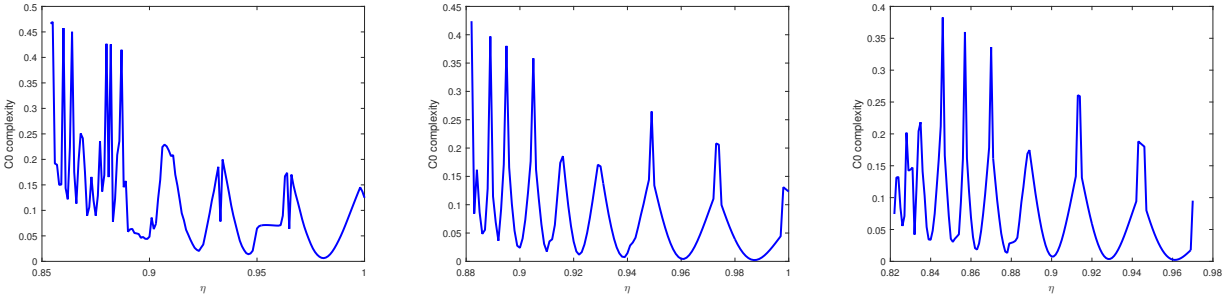

(a) **(b)** **(c)**

Figure 11. C_0 complexity of (2.5) versus κ with IC=(0.4, 0.4, 0.2): for (a) $\eta = 1.9, \mu = 2.1$; (b) $\eta = 2, \mu = 2$; (c) $\eta = 1.9$, and $\mu = 1.98$.

For comparative analysis, Figure 12 also provides the Permutation Entropy (PE) results for the discrete fractional-order computer virus model (2.5), with consistent parameter ranges $\sigma = 0.1, \alpha_1 = 0.1$, and $\alpha_2 = 0.3$. Figure 12(a) details the findings when $\eta = 1.9, \mu = 2.1$. Figure 12(b) corresponds to the scenario where $\eta = 2, \mu = 2$, contrasting with Figure 12(c) which depicts the case for $\eta = 1.9, \mu = 1.98$. These PE results demonstrate the model's high sensitivity to parameter adjustments, with entropy levels indicating chaotic or stable states, which corroborates findings from Lyapunov Exponent studies.

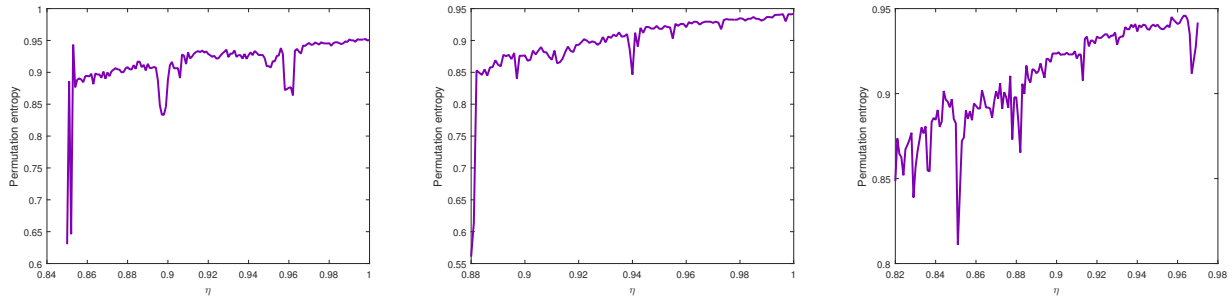

(a) **(b)** **(c)**

Figure 12. Permutation Entropy of (2.5) versus κ with IC=$(0.4, 0.4, 0.2)$: for (a) $\eta = 1.9, \mu = 2.1$; (b) $\eta = 2, \mu = 2$; (c) $\eta = 1.9$, and $\mu = 1.98$.

Table 1 reports the numerical complexity analysis for the proposed, discrete, fractional-order computer virus model. The values of ApEn, PE, and C_0 confirm that the system exhibits significant complexity and unpredictable behavior, which are desirable properties in the context of secure modeling and chaos-based systems.

Table 1. C_0, and PE of the fractional discrete system (2.5) for $\sigma = 0.1, \alpha_1 = 0.1$, and $\alpha_2 = 0.3$.

Control parameters	ApEn	C_0	PE
$(\eta, \mu, \kappa) = (1.9, 2.1, 0.862)$	0.42304	0.45551	0.61046
$(\eta, \mu, \kappa) = (2, 2, 0.8821)$	0.3429	0.42724	0.56363
$(\eta, \mu, \kappa) = (1.9, 1.98, 0.823)$	0.32958	0.43613	0.55241
$(\eta, \mu, \kappa) = (1.2, 2.1, 0.499)$	0.67287	0.48425	0.70189

6. Chaos control methods

In this section, we cover the control and synchronization scheme of the fractional discrete system (2.5). Control mechanisms play a crucial role in stabilizing chaotic systems and ensuring predictable behavior, especially in real-world applications where instability can lead to undesirable outcomes. By introducing control parameters, we can influence the system's dynamics, regulating bifurcations and steering it toward desired states. This is especially significant for synchronization, where multiple systems must remain coordinated, such as in secure communications. Effective control strategies help mitigate chaos, making the system more reliable and functional. In this section, nonlinear controllers are introduced to achieve stability and synchronization in the fractional discrete computer virus model.

6.1. Stabilization of fractional discrete computer virus model

Chaos control techniques like Sliding Mode Control (SMC) and Adaptive Control are widely used. SMC is robust but suffers from chattering, while Adaptive Control, used in this study, adjusts in real-time to system dynamics, offering flexibility in uncertain environments. Although computationally

intensive, Adaptive Control provides a more accurate representation of chaotic behavior, making it ideal for real-time applications like cybersecurity, where quick adjustments are vital to address evolving threats. A stabilizing control mechanism is introduced to regulate the behavior of the proposed fractional chaotic model (2.5). The primary goal is to develop an adaptive control mechanism that ensures every state the system has, converge to a fixed point over time. This is achieved by applying the stability theorem for fractional maps 2. The controlled form of (2.5) is expressed by:

$$\begin{cases} {}^{\mathtt{c}}\Delta_{\mathtt{a}}^{\kappa} S(\mathtt{t}) = \sigma - \mu S(\rho)(L(\rho) + B(\rho)) + \alpha_1 L(\rho) + \alpha_2 B(\rho) - \sigma S(\rho) + C_1(\rho), \\ {}^{\mathtt{c}}\Delta_{\mathtt{a}}^{\kappa} L(\mathtt{t}) = \mu S(\rho)(L(\rho) + B(\rho)) - \alpha_1 L(\rho) - \eta L(\rho) - \sigma L(\rho) + C_2(\rho), \\ {}^{\mathtt{c}}\Delta_{\mathtt{a}}^{\kappa} B(\mathtt{t}) = \eta L(\rho) - \alpha_2 B(\rho) - \sigma B(\rho) + C_3(\rho). \end{cases} \tag{6.1}$$

Where Here, $C = (C_1, C_2, C_3)^T$ represents the adaptive controller. The theorem stated hereafter presents control laws designed to stabilize the newly offered fractional computer virus model.

Theorem 3. *If appropriate control laws are formulated hereinafter*

$$\begin{cases} C_1(\rho) = \mu S(\rho)(L(\rho) + B(\rho)) - \alpha_1 L(\rho) - \alpha_2 B(\rho) + c_1(S_0 - S(\rho)), \\ C_2(\rho) = -\mu S(\rho)(L(\rho) + B(\rho)) + c_2(L_0 - L(\rho)), \\ C_3(\rho) = -\eta L(\rho) + c_3(B_0 - B(\rho)), \end{cases} \tag{6.2}$$

where $0 \leq c_1 + \sigma \leq 2^{\kappa}$, $0 \leq c_2 + \alpha_1 + \eta + \sigma \leq 2^{\kappa}$, $0 \leq c_3 + \alpha_2 + \sigma \leq 2^{\kappa}$, and $S_0 = 1, L_0 = 0, B_0 = 0$, then the fractional computer virus system can be successfully brought to stability at its equilibrium point.

Proof. By substituting C_1, C_2, C_3, into (6.1), the following system is derived

$${}^{\mathtt{c}}\Delta_{\mathtt{a}}^{\kappa} X(\mathtt{t}) = \mathcal{K} X(\rho), \tag{6.3}$$

such that $X(\mathtt{t}) = (S, L, B)^T$,

$$\begin{cases} {}^{\mathtt{c}}\Delta_{\mathtt{a}}^{\kappa} S(\mathtt{t}) &= \sigma + c_1 - (\sigma + c_1) S(\rho), \\ {}^{\mathtt{c}}\Delta_{\mathtt{a}}^{\kappa} L(\mathtt{t}) &= -(c_2 + \alpha_1 + \eta + \sigma) L(\rho), \\ {}^{\mathtt{c}}\Delta_{\mathtt{a}}^{\kappa} B(\mathtt{t}) &= -(c_3 + \alpha_2 + \sigma) B(\rho), \end{cases} \tag{6.4}$$

and

$$\mathcal{K} = \begin{pmatrix} -(c_1 + \sigma) & 0 & 0 \\ 0 & -(c_2 + \alpha_1 + \eta + \sigma) & 0 \\ 0 & 0 & -(c_3 + \alpha_2 + \sigma) \end{pmatrix}, \tag{6.5}$$

for the parameter values leading to chaos $\eta = 1.2$, $\mu = 2.1$, $\sigma = 0.1$, $\alpha_1 = 0.1$, and $\alpha_2 = 0.6$, we found that the proper values of $\mathcal{K}$ satisfy the stability requirement of Theorem 2 for $0 \leq c_1 + \sigma \leq 2^{\kappa}$, $0 \leq c_2 + \alpha_1 + \eta + \sigma \leq 2^{\kappa}$, and $0 \leq c_3 + \alpha_2 + \sigma \leq 2^{\kappa}$. □

To confirm the validity of Theorem 3, running simulations were conducted such that $c_1 = 0.9, c_2 = -0.4$, and $c_3 = 0.3$. Figures 13 visualize the time-domain response of the controlled fractional discrete computer virus model (6.1). The figures show that the system's states converge to the virus-free fixed point asymptotically, confirming the effectiveness of the stabilization method. In this study, our

focus was on demonstrating the effectiveness of control and synchronization strategies via numerical simulations. A complete theoretical design and stability analysis are beyond the current scope but are planned as an important direction for future work.

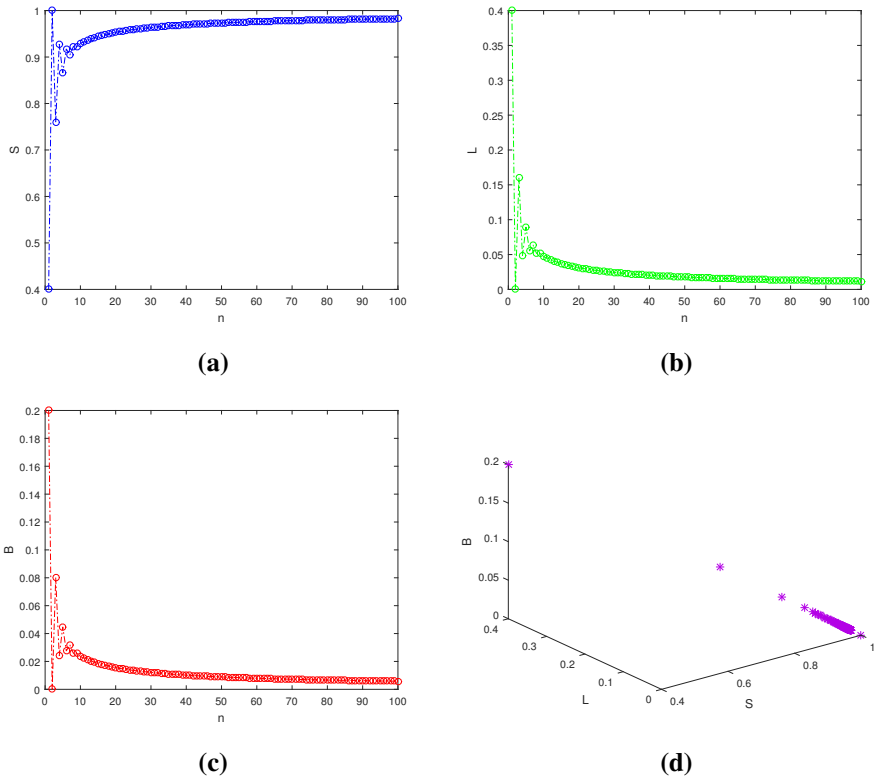

(a) **(b)** **(c)** **(d)**

Figure 13. Stabilized states of the controlled fractional discrete computer virus model (6.1) with $\kappa = 0.6$.

6.2. Synchronization scheme

Several synchronization methods exist for chaotic systems, such as Pecora-Carroll and projection synchronization, each suited to different system structures. Compared to these, the nonlinear control-based approach used here offers greater flexibility for handling fractional discrete dynamics and enables tailored controller design. Future comparisons may help optimize synchronization in cybersecurity applications. The subsequent discussion focuses on the development of nonlinear controllers for the synchronization of the fractional discrete computer virus model (2.5). The synchronization procedure tries to eliminate the discrepancy between a master map, represented by Equation (2.5), and a slave map, thus achieving convergence to zero error. The slave map is formally defined as:

$$\begin{cases} {}^{c}\Delta_{a}^{\kappa} S_s(t) = \sigma - \mu S_s(\rho)(L_s(\rho) + B_s(\rho)) + \alpha_1 L_s(\rho) + \alpha_2 B_s(\rho) - \sigma S_s(\rho) + T_1(\rho), \\ {}^{c}\Delta_{a}^{\kappa} L_s(t) = \mu S_s(\rho)(L_s(\rho) + B_s(\rho)) - \alpha_1 L_s(\rho) - \eta L_s(\rho) - \sigma L_s(\rho) + T_2(\rho), \\ {}^{c}\Delta_{a}^{\kappa} B_s(t) = \eta L_s(\rho) - \alpha_2 B_s(\rho) - \sigma B_s(\rho) + T_3(\rho). \end{cases} \tag{6.6}$$

T_1, T_2, T_3 denote the controllers for synchronization. The fractional error system is formulated as detailed below:

$$\begin{cases} {}^{\mathrm{c}}\Delta_{\mathrm{a}}^{\kappa} e_1(\mathtt{t}) & = -\mu S_s(\rho)(L_s(\rho) + B_s(\rho)) + \mu S(\rho)(L(\rho) + B(\rho)) + \alpha_1 e_2(\rho) + \alpha_2 e_3(\rho) \\ & \quad -\sigma e_1(\rho) + T_1(\rho), \\ {}^{\mathrm{c}}\Delta_{\mathrm{a}}^{\kappa} e_2(\mathtt{t}) & = -\mu S_s(\rho)(L_s(\rho) + B_s(\rho)) + \mu S(\rho)(L(\rho) + B(\rho)) - (\alpha_1 + \eta + \sigma) e_2(\rho) + T_2(\rho), \\ {}^{\mathrm{c}}\Delta_{\mathrm{a}}^{\kappa} e_3(\mathtt{t}) & = \eta e_2(\rho) - (\alpha_2 + \sigma) e_3(\rho) + T_3(\rho). \end{cases} \tag{6.7}$$

The synchronization scheme's control rule is detailed in the following theorem

Theorem 4. *Subject to*

$$\begin{cases} T_1(\rho) = \mu S_s(\rho)(L_s(\rho) + B_s(\rho)) - \mu S(\rho)(L(\rho) + B(\rho)) - \alpha_1 e_2(\rho) - \alpha_2 e_3(\rho) + t_1 e_1(\rho), \\ T_2(\rho) = -\mu S_s(\rho)(L_s(\rho) + B_s(\rho)) + \mu S(\rho)(L(\rho) + B(\rho)) + t_2 e_2(\rho), \\ T_3(\rho) = -\eta e_2(\rho) + t_3 e_3(\rho), \end{cases} \tag{6.8}$$

then, the master and slave computer virus models, represented by (2.5) and (6.6), achieve synchronization, where $\sigma - 2^{\kappa} \leq t_1 \leq \sigma$, $\alpha_1 + \eta + \sigma - 2^{\kappa} \leq t_2 \leq \alpha_1 + \eta + \sigma$, $\alpha_2 + \sigma - 2^{\kappa} \leq t_3 \leq \alpha_2 + \sigma$.

Proof. Substituting control law (6.8) into error map (6.7) results

$${}^{\mathrm{c}}\Delta_{\mathrm{a}}^{\kappa}(e_1(\mathtt{t}), e_2(\mathtt{t}), e_3(\mathtt{t}))^T = \mathcal{N}(e_1(\rho), e_2(\rho), e_3(\rho))^T, \tag{6.9}$$

where

$$\mathcal{N} = \begin{pmatrix} t_1 - \sigma & 0 & 0 \\ 0 & t_2 - \alpha_1 - \eta - \sigma & 0 \\ 0 & 0 & t_3 - \alpha_2 - \sigma \end{pmatrix}. \tag{6.10}$$

The eigenvalues of matrix $\mathcal{N}$ are given by $\lambda_1 = t_1 - \sigma, \lambda_2 = t_2 - \alpha_1 - \eta - \sigma$, and $\lambda_3 = t_3 - \alpha_2 - \sigma$, these eigenvalues fulfill the stability criteria defined in Theorem 2 when $\sigma - 2^{\kappa} \leq t_1 \leq \sigma$, $\alpha_1 + \eta + \sigma - 2^{\kappa} \leq t_2 \leq \alpha_1 + \eta + \sigma$, $\alpha_2 + \sigma - 2^{\kappa} \leq t_3 \leq \alpha_2 + \sigma$. This confirms that the fractional error map (6.7) demonstrates asymptotic stability at the origin. Consequently, synchronization is attained between the driving model (2.5) and the driven model (6.6). □

Numerical simulations in MATLAB were executed to confirm the authenticity of the derived synchronization result. With parameters set to $\eta = 1.2$, $\mu = 2.1$, $\sigma = 0.1$, $\alpha_1 = 0.1$, $\alpha_2 = 0.6$, $t_1 = -0.9, t_2 = 0.4, t_3 = -0.3$, and $\kappa = 0.6$, and initial error values $(e_1(0), e_2(0), e_3(0)) = (0.1, -0.2, -0.1)$, the progression of the fractional error system (6.7) is illustrated in Figure 14. As is apparent from the figure, the error states diminish to zero, thus validating the previously described synchronization process.

The control approach proposed in this study relies on full-state feedback, meaning all system states must be measurable. Although this is commonly used in theoretical work, in practical scenarios, it may not always be feasible. In future work, we plan to explore observer-based or output-feedback control strategies to overcome this limitation and make the model more applicable to real-world systems.

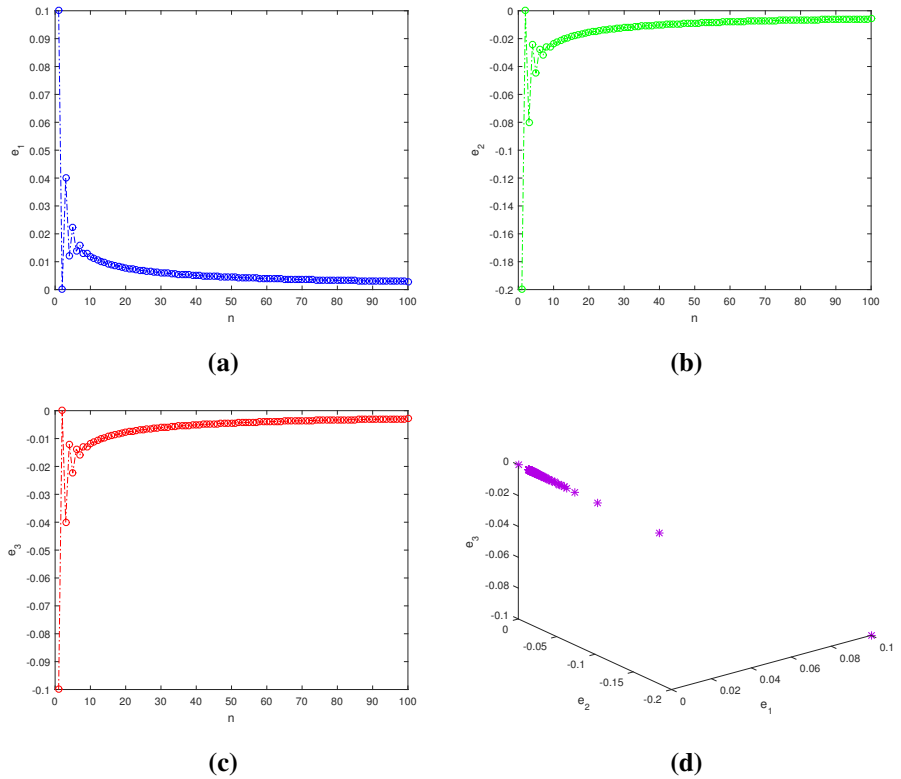

Figure 14. Error synchronization states.

7. Conclusions

In this study, we developed and analyzed a discrete fractional-order computer virus model to investigate its dynamical properties, stability conditions, and chaotic behavior. Using the basic reproduction number R_0, we established stability thresholds and identified conditions for chaos, confirmed by bifurcation analysis and Lyapunov exponents. Complexity metrics (Approximate Entropy, C_0 Complexity, and Permutation Entropy), further quantified the system's unpredictability, revealing how fractional-order parameters drive transitions between equilibrium, periodic oscillations, and chaos. These results underscore the importance of fractional calculus in modeling virus propagation, where memory effects and non-local dynamics influence infection spread and persistence. However, while the fractional order parameter κ critically governs the system's memory effects and dynamic behavior, we do not address methods to estimate κ from real-world data. Parameter estimation for fractional-order models remains a complex challenge due to the models' nonlocal and memory-dependent nature. Future research should focus on developing robust identification techniques, such as optimization-based fitting or machine learning approaches, to infer κ from empirical data. Such efforts will enhance the practical applicability and validation of fractional-order models in cybersecurity contexts.

The chaotic behavior observed in the virus propagation model offers novel insights for cybersecurity. By leveraging the inherent unpredictability of chaotic systems, adaptive defense strategies could dynamically counteract evolving threats. For example, chaotic signatures might inform algorithms designed to detect irregular propagation dynamics, enhancing anomaly detection in

Intrusion Detection Systems (IDS) or adaptive firewalls. Furthermore, our successful implementation of control and synchronization techniques demonstrates that chaotic systems can be stabilized or coordinated under tailored control laws. This capability is critical for real-time threat mitigation, enabling synchronized defenses across networked systems.

The integration of fractional-order control with hardware (e.g., microcontrollers, FPGAs) could enable real-time cybersecurity applications, such as adaptive intrusion detection or secure communication systems. Recent advancements in chaotic systems such as 3D memristive maps for image encryption or chaotic neuron-based models like the 2D Logistic-Rulkov Neuron Map demonstrate the versatility of chaos in cybersecurity. Similarly, the chaotic dynamics of our fractional-order virus model could inspire secure data transmission protocols or adaptive defense strategies in networked environments. Future work should prioritize practical deployment, leveraging hardware-software synergies to enhance threat mitigation in real-world systems.

Overall, we establish a foundation for fractional-order modeling in cybersecurity. In future investigations, researchers could explore the influence of additional fractional parameters, optimize control strategies, and extend the model to real-world scenarios. Further research should prioritize data-driven estimation of the fractional order to bridge theoretical models with empirical threat patterns, ensuring robust validation in operational cybersecurity frameworks. By merging fractional calculus with chaotic systems, this work paves the way for resilient, adaptive cybersecurity frameworks capable of countering sophisticated threats.

Author contributions

Omar Kahouli: Methodology, funding acquisition, project administration, validation; Imane Zouak: Conceptualization, methodology, software, formal analysis, data curation, writing original draft preparation, writing review and editing, investigation, visualization; Ma'mon Abu Hammad: Project administration, funding acquisition, visualization, resources; Adel Ouannas: Conceptualization, supervision, project administration, visualization, resources, validation. All authors have read and approved the final version of the manuscript for publication.

Use of Generative-AI tools declaration

The authors declare that they has not used Artificial Intelligence (AI) tools in the creation of this article.

Conflicts of interest

The authors declare that they have no conflict of interest.

References

1. P. Szor, *The art of computer virus research and defense*, Boston: Addison-Wesley Professional, 2005.
2. F. Cohen, Computer viruses: theory and experiments, *Comput. Secur.*, **6** (1987), 22–35. https://doi.org/10.1016/0167-4048(87)90122-2

3. L.-X. Yang, X. F. Yang, The spread of computer viruses under the influence of removable storage devices, *Appl. Math. Comput.*, **219** (2012), 3914–3922. https://doi.org/10.1016/j.amc.2012.10.027
4. J. O. Kephart, S. R. White, Directed-graph epidemiological models of computer viruses, *The 1991 IEEE Computer Society Symposium on Research in Security and Privacy*, Oakland, CA, USA, 1991, 343–359. https://doi.org/10.1109/RISP.1991.130801
5. W. H. Murray, The application of epidemiology to computer viruses, *Comput. Secur.*, **7** (1988), 139–145. https://doi.org/10.1016/0167-4048(88)90327-6
6. X. F. Yang, L.-X. Yang, Towards the epidemiological modeling of computer viruses, *Discrete Dyn. Nat. Soc.*, **2012** (2012), 259671. https://doi.org/10.1155/2012/259671
7. H. R. Biswas, M. M. Hasan, S. K. Bala, Chaos theory and its applications in our real life, *Barishal University Journal Part 1*, **5** (2018), 123–140.
8. L. M. Pecora, T. L. Carroll, G. A. Johnson, D. J. Mar, J. F. Heagy, Fundamentals of synchronization in chaotic systems: concepts and applications, *Chaos*, **7** (1997), 520–543. https://doi.org/10.1063/1.166278
9. H. R. Lin, C. H. Wang, S. C. Du, W. Yao, Y. C. Sun, A family of memristive multibutterfly chaotic systems with multidirectional initial-based offset boosting, *Chaos Soliton. Fract.*, **172** (2023), 113518. https://doi.org/10.1016/j.chaos.2023.113518
10. D. X. Yang, Z. J. Liu, J. L. Zhou, Chaos optimization algorithms based on chaotic maps with different probability distribution and search speed for global optimization, *Commun. Nonlinear Sci.*, **19** (2014), 1229–1246. https://doi.org/10.1016/j.cnsns.2013.08.017
11. S. Gao, J. F. Liu, H. H.-C. Iu, U. Erkan, S. Zhou, R. Wu, et al., Development of a video encryption algorithm for critical areas using 2D extended Schaffer function map and neural networks, *Appl. Math. Model.*, **134** (2024), 520–537. https://doi.org/10.1016/j.apm.2024.06.016
12. S. Gao, R. Wu, X. Y. Wang, J. F. Liu, Q. Li, X. L. Tang, EFR-CSTP: Encryption for face recognition based on the chaos and semi-tensor product theory, *Inform. Sciences*, **621** (2023), 766–781. https://doi.org/10.1016/j.ins.2022.11.121
13. G.-C. Wu, D. Baleanu, Discrete fractional logistic map and its chaos, *Nonlinear Dyn.*, **75** (2014), 283–287. https://doi.org/10.1007/s11071-013-1065-7
14. A. Ouannas, I. M. Batiha, V.-T. Pham, *Fractional discrete chaos: theories, methods and applications*, Singapore: World Scientific, 2023. https://doi.org/10.1142/13277
15. M. T. Shatnawi, N. Djenina, A. Ouannas, I. M. Batiha, G. Grassi, Novel convenient conditions for the stability of nonlinear incommensurate fractional-order difference systems, *Alex. Eng. J.*, **61** (2022), 1655–1663. https://doi.org/10.1016/j.aej.2021.06.073
16. A. Abbes, A. Ouannas, N. Shawagfeh, A. A. Khennaoui, Incommensurate fractional discrete neural network: chaos and complexity, *Eur. Phys. J. Plus*, **137** (2022), 235. https://doi.org/10.1140/epjp/s13360-022-02472-6
17. L. Diabi, A. Ouannas, G. Grassi, S. Momani, Symmetry breaking in fractional difference chaotic equations and their control, *Symmetry*, **17** (2025), 352. https://doi.org/10.3390/sym17030352

18. R. Saadeh, A. Abbes, A. Al-Husban, A. Ouannas, G. Grassi, The fractional discrete predator-prey model: chaos, control, and synchronization, *Fractal Fract.*, **7** (2023), 120. https://doi.org/10.3390/fractalfract7020120

19. A. Abbes, A. Ouannas, N. Shawagfeh, H. Jahanshahi, The fractional-order discrete COVID-19 pandemic model: stability and chaos, *Nonlinear Dyn.*, **111** (2023), 965–983. https://doi.org/10.1007/s11071-022-07766-z

20. A.-A. Khennaoui, A. Ouannas, S. Bendoukha, X. Wang, V.-T. Pham, On chaos in the fractional-order discrete-time unified system and its control synchronization, *Entropy*, **20** (2018), 530. https://doi.org/10.3390/e20070530

21. A. Ouannas, G. Grassi, A. T. Azar, A. A. Khennaouia, V. T. Pham, Chaotic control in fractional-order discrete-time systems, In: *Proceedings of the International Conference on Advanced Intelligent Systems and Informatics 2019*, Cham: Springer, 2019, 207–217. https://doi.org/10.1007/978-3-030-31129-2_20

22. M. A. Hammad, R. Alkhateeb, G. Farraj, N. Djenina, A. Ouannas, Discrete fractional incommensurate order Ebola model: analyzing dynamics and numerical simulation, *Fractals*, **2025** (2025), 2540127. https://doi.org/10.1142/S0218348X25401279

23. A. A. Khennaoui, V. T. Pham, V. P. Thoai, A. Ouannas, G. Grassi, S. Momani, From Lozi map to fractional memristive Lozi map, *Eur. Phys. J. Spec. Top.*, **232** (2023), 2385–2393. https://doi.org/10.1140/epjs/s11734-023-00911-8

24. A. Abbes, A. Ouannas, N. Shawagfeh, An incommensurate fractional discrete macroeconomic system: bifurcation, chaos, and complexity, *Chinese Phys. B*, **32** (2023), 030203. https://doi.org/10.1088/1674-1056/ac7296

25. A. Dababneh, N. Djenina, A. Ouannas, G. Grassi, I. M. Batiha, I. H. Jebril, A new incommensurate fractional-order discrete COVID-19 model with vaccinated individuals compartment, *Fractal Fract.*, **6** (2022), 456. https://doi.org/10.3390/fractalfract6080456

26. A. Abbes, A. Ouannas, A. Hioual, S. Momani, Hidden chaos in a new memristor-based discrete system with commensurate, incommensurate and variable fractional orders, *Phys. Scr.*, **99** (2024), 105233. https://doi.org/10.1088/1402-4896/ad7361

27. A. Ouannas, S. Ahmed, G. Grassi, M. Al Horani, A. A. Khennaoui, A. Hioual, The fractional variable-order Grassi–Miller map: chaos, complexity, and control, *Comput. Math. Methods*, **2025** (2025), 6674521. https://doi.org/10.1155/cmm4/6674521

28. S. Gao, H. H.-C. Iu, U. Erkan, C. Simsek, A. Toktas, Y. H. Cao, et al., A 3D memristive cubic map with dual discrete memristors: design, implementation, and application in image encryption, *IEEE T. Circ. Syst. Vid.*, **2025** (2025), 3545868. https://doi.org/10.1109/TCSVT.2025.3545868

29. S. Gao, Z. Y. Zhang, H. H.-C. Iu, S. Q. Ding, J. Mou, U. Erkan, et al., A parallel color image encryption algorithm based on a 2-D Logistic-Rulkov neuron map, *IEEE Internet Things*, **12** (2025), 18115–18124. https://doi.org/10.1109/JIOT.2025.3540097

30. J. G. Ren, X. F. Yang, Q. Y. Zhu, L.-X. Yang, C. M. Zhang, A novel computer virus model and its dynamics, *Nonlinear Anal.-Real*, **13** (2012), 376–384. https://doi.org/10.1016/j.nonrwa.2011.07.048

31. Z. X. Hu, H. W. Wang, F. C. Liao, W. B. Ma, Stability analysis of a computer virus model in latent period, *Chaos Soliton. Fract.*, **75** (2015), 20–28. https://doi.org/10.1016/J.CHAOS.2015.02.001

32. O. Kahouli, I. Zouak, A. Ouannas, I. Abidi, Y. Bahou, S. Elgharbi, et al., Control and synchronization of chaos in some fractional computer virus models, *Asian J. Control*, **2025** (2025), 3693. https://doi.org/10.1002/asjc.3693

33. T. Abdeljawad, On Riemann and Caputo fractional differences, *Comput. Math. Appl.*, **62** (2011), 1602–1611. https://doi.org/10.1016/j.camwa.2011.03.036

34. F. M. Atici, P. Eloe, Discrete fractional calculus with the nabla operator, *Electron. J. Qual. Theory Differ. Equ.*, **2009** (2009), 1–12. https://doi.org/10.14232/ejqtde.2009.4.3

35. J. Čermák, I. Győri, L. Nechvátal, On explicit stability conditions for a linear fractional difference system, *Fract. Calc. Appl. Anal.*, **18** (2015), 651–672. https://doi.org/10.1515/fca-2015-0040

36. L.-X. Yang, X. F. Yang, Q. Y. Zhu, L. S. Wen, A computer virus model with graded cure rates, *Nonlinear Anal.-Real*, **14** (2013), 414–422. https://doi.org/10.1016/j.nonrwa.2012.07.005

37. R. Mahardika, Widowati, Y. D. Sumanto, Routh-Hurwitz criterion and bifurcation method for stability analysis of tuberculosis transmission model, *J. Phys.: Conf. Ser.*, **1217** (2019), 012056. https://doi.org/10.1088/1742-6596/1217/1/012056

38. G.-C. Wu, D. Baleanu, Jacobian matrix algorithm for Lyapunov exponents of the discrete fractional maps, *Commun. Nonlinear Sci.*, **22** (2015), 95–100. https://doi.org/10.1016/j.cnsns.2014.06.042

39. J. S. Richman, J. R. Moorman, Physiological time-series analysis using approximate entropy and sample entropy, *Am. J. Physiol.-Heart C.*, **278** (2000), H2039–H2049. https://doi.org/10.1152/ajpheart.2000.278.6.H2039

40. E.-H. Shen, Z.-J. Cai, F.-J. Gu, Mathematical foundation of a new complexity measure, *Appl. Math. Mech.*, **26** (2005), 1188–1196. https://doi.org/10.1007/BF02507729

41. C. Bandt, B. Pompe, Permutation entropy: A natural complexity measure for time series, *Phys. Rev. Lett.*, **88** (2002), 174102. http://doi.org/10.1103/PhysRevLett.88.174102

AIMS Press